Cooperative CO₂ Scission by Anomalous Insertion into a Rh-Si Bond

Matthew T. Whited,**,† Jia Zhang,† Theodore M. Donnell,† Vanessa H. Eng,§ Paul O. Peterson,† Michael J. Trenerry,† Daron E. Janzen,‡ and Buck L. H. Taylor*,†,§

- † Department of Chemistry, Carleton College, Northfield, MN 55057, United States
- Department of Chemistry and Biochemistry, St. Catherine University, St. Paul, Minnesota 55105, United States
- § Department of Chemistry, University of Portland, Portland, OR 97203, United States

ABSTRACT: Pincer-type [P_2Si]Rh complexes featuring a rhodium–silicon bond are shown to facilitate well-defined stoichiometric reductions of CO_2 with Si–O bond formation by two different pathways: (a) hydride transfer to CO_2 followed by formate migration to silicon, or (b) complete scission of the C=O bond at the Rh–Si unit to afford a product with siloxide and carbonyl ligands. A combined experimental and computational study shows that the latter process occurs by anomalous insertion of CO_2 into the polarized Rh^{δ} – $Si^{\delta+}$ bond, a finding that is confirmed by extending the reactivity to an unchelated system. The siloxide carbonyl product can be further elaborated by reaction with water or pinacolborane to give structurally distinct CO_2 reduction products. Taken together, these results demonstrate how metal/main-group bonds can be tuned to direct migratory insertion reactivity.

INTRODUCTION

Small-molecule oxygenates such as carbon dioxide, carbon monoxide, and nitrous oxide represent appealing targets for catalytic transformation due to their high stability, ready availability, and roles as pollutants and/or greenhouse gases. CO₂ in particular represents a ubiquitous and potentially useful C₁ source, so significant efforts have been invested in devising new strategies for its modification. In spite of its stability and high C=O bond strength, the $C^{\delta+}=O^{\delta-}$ bond polarization renders it susceptible to synergistic activation, e.g., in the 1,2-addition of maingroup frustrated Lewis pairs (FLPs) to the C=O bond. Although FLPs represent a recent area of intense study, these transformations closely resemble migratory insertions that are a ubiquitous in organometallic chemistry (Figure 1),² where normal insertions to give metal carboxylates are by far the most common as a predictable consequence of the $M^{\delta^{\perp}} - X^{\delta^{\perp}}$ polarization of the bonds.3

We have been exploring whether metal-silicon single and multiple bonds, incorporated as central units in a pincer-type [P₂Si] scaffold, can be used to access new biphilic modes for cooperative small-molecule activation, akin to FLPs.4 In such a context, so-called "anomalous" insertions of CO2 exhibiting a reversed regiochemical preference are appealing reaction targets (Figure 1), since an electronegative metal and electropositive silicon might be tuned to reveal a $M^{\delta-}$ -Si $^{\delta+}$ facade for substrate activation. Migratory insertions of CO₂ into metal-silicon bonds are known,5 yet all reported examples of well-defined insertions of CO₂ follow the normal pathway in spite of the wellknown oxophilicity of silicon and the propensity of aldehydes and ketones to insert into M-Si in anomalous fashion.^{6,7} In this contribution, we show a pathway for CO₂ scission and further elaboration initiated by anomalous insertion into a Rh-Si bond and explore the electronic characteristics that engender such reactivity.

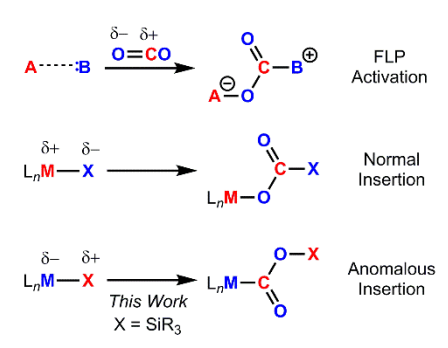


Figure 1. FLP and migratory insertion approaches to CO₂ activation

RESULTS

CO₂ Insertion into an Si–H Bond at [P₂Si]Rh. Several years ago, we reported that the pincer-type complex [CyP₂Si^{OTf}]Rh(nbd) (1-OTf) featuring a central triflatosilyl donor undergoes facile Si–OTf cleavage, rearranging in the presence of H₂ to a hydrosilyl product, [CyP₂Si^H]Rh(H)(OTf) (2-OTf), formally splitting H₂ across the Rh–Si bond. Once activated in this way, H₂ can be transferred to strained alkenes, regenerating the triflatosilyl starting material (Scheme 1). 4c Catalytic alkene hydrogenation was investigated, though Rh/Si cooperation was not implicated in the catalytic process.

Given the high oxophilicity of silicon, we wondered whether a highly fluxional system such as **2-OTf** might afford new routes to functionalization of oxygen-containing molecules, namely CO₂. Indeed, exposure of **2-OTf** to CO₂ (1 atm) results in net insertion of CO₂ into the Si–H bond, giving formatosilyl complex **3-OTf** (Scheme 2) in addition to a minor product (**6-OTf**, *vide infra*). Although we were unable to crystallize **3-OTf**, its identity was corroborated by an independent synthesis from formic acid as well as its numerous spectroscopic handles, including a prominent infrared (IR) band associated with the for-

mate carbonyl ($v_{CO} = 1697 \text{ cm}^{-1}$) and ^{1}H NMR hydride resonance ($\delta - 23.00 \text{ ppm}$ (dt, $^{1}J_{\text{RhH}} = 32.7 \text{ Hz}$, $^{2}J_{\text{PH}} = 13.2 \text{ Hz}$)) quite similar to that of **2-OTf** and related complexes.

Scheme 1. Cooperative H_2 activation and transfer with $\lceil^{Cy}P_2Si^{OTf}\rceil Rh^{4c}$

We envisioned two general pathways through which **3-OTf** could form, distinguished by whether hydride transfer to CO₂ involves silicon assistance (Scheme 2):

- (a) CO₂ inserts at Rh–H to make a rhodium formate complex that rearranges to place the formate on silicon, or
- (b) Rearrangement of **2-OTf** via α-H migration unmasks a highly Lewis-acidic silicon with proximal Rh–H, allowing silylene-assisted hydride transfer to CO₂ and affording **3-OTf** directly.

Scheme 2. Possible mechanisms for CO₂ insertion into Si–H of **2-OTf**

Mechanism (a) would be consistent with a previous reports showing CO₂ reduction by pincer-type RhH₂ complexes where metal/ligand cooperation is not implicated⁸ as well as studies of alkene hydrogenation by [P₂Si]Rh complexes.^{4c,9} Mechanism (b) would closely resemble recent findings from our group showing silylene-assisted hydride transfer to CO₂ at ruthenium^{4b} and would feature an intermediate that is structurally analogous to a rhodium silylene previously proposed by Milstein.¹⁰ To distinguish between mechanisms, we added CO₂ (1 atm) to our recently reported dihydrogen complex, [CyP₂Si^{Me}]Rh(H₂) (4-CH₃), which features a robust Si–CH₃ bond rather than the labile Si–H. The complex reacts instantly

to give the hydrido formate complex 5-CH₃ (eq 1), strongly suggesting by analogy that CO₂ insertion at complex 2-OTf does not require silicon assistance and occurs via mechanism (a).

Rh/Si Cooperative Scission of CO₂: Experimental Findings. Although hydride transfer to CO₂ did not implicate Rh/Si cooperation, we consistently observed a minor byproduct (6-OTf) during reaction of 2-OTf with CO₂ indicating loss of H₂ and cleavage of the Si–Rh bond (as evidenced by an upfield ²⁹Si NMR shift exhibiting no ²⁹Si/¹⁰³Rh coupling). Complex 6-OTf could be cleanly obtained by reaction of the norbornadiene (nbd) adduct 1-OTf with CO₂ in dichloromethane. In this case, formation of 6-OTf is accompanied by expulsion of nbd.

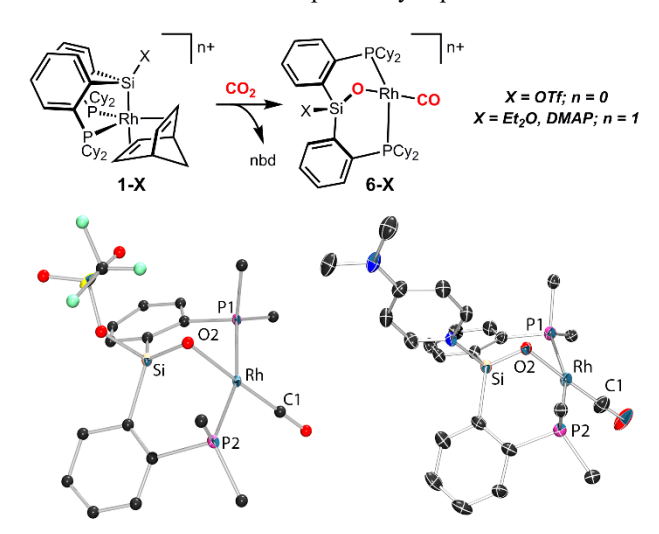


Figure 2. Deoxygenation of CO₂ by complexes **1-X** and molecular structures of siloxide complexes **6-OTf** (left) and **6-DMAP**⁺ (right) with hydrogen atoms, co-crystallized solvents, and counterions removed and phosphine substituents truncated for clarity (isotropically refined atoms of **6-OTf** shown as spheres, anisotropically refined atoms rendered as 50% probability thermal ellipsoids). Selected bond lengths (Å) and angles (deg) for **6-OTf**: Rh–C1, 1.86(3); Rh–O2, 2.10(2); Si–O2, 1.552(18); O2–Rh–C1, 177.8(9); P1–Rh–P2, 162.1(2); Si–O2–Rh, 100.2(9). For **6-DMAP**⁺: Rh–C1, 1.822(7); Rh–O2, 2.057(3); Si–O2, 1.579(4); O2–Rh–C1, 177.3(3); P1–Rh–P2, 160.24(6); Si–O2–Rh, 105.7(2).

Complex **6-OTf** was identified by a variety of spectroscopic methods as the siloxide pincer complex $[^{\text{Cy}}_{\text{P}}\text{Si}^{(\text{OTf})(\mu-\text{O})}]\text{Rh}(\text{CO}),^{11}$ the product of CO₂ scission at the Si–Rh bond (Figure 2). As noted above, the upfield shift of the ^{29}Si NMR signal (δ –42.1 ppm ($^3J_{\text{SiP}}=7.5$ Hz)), combined with a lack of $^{29}\text{Si}^{/103}\text{Rh}$ coupling, strongly indicated a loss of the Si–Rh bond. IR spectroscopy showed a prominent metal carbonyl stretching mode ($v_{\text{CO}}=1955$ cm⁻¹). The ^{13}C -labelled isotopologue **6-OTf**- ^{13}C , prepared from $^{13}\text{CO}_2$, exhibited a 45 cm⁻¹ red shift ($v_{\text{CO}}=1910$ cm⁻¹ (1912 cm⁻¹ predicted)) relative to **6-OTf** and a prominent Rh– \underline{C} O NMR signal (δ 194.3 ppm (dt, $^1J_{\text{RhC}}=$

71.9 Hz, ${}^{2}J_{PC} = 13.0$ Hz)). After numerous crystallization attempts, a low-quality crystal structure of **6-OTf** was obtained (Figure 2). Although the low quality of the structure precluded anisotropic refinement of atoms other than Rh, P, Si, and S, the connectivity was established. A subsequent high-quality structure of **6-DMAP**⁺ (Figure 2, *vide infra*) also provides strong support for the formulation presented.

Complex 6-OTf features a square-planar Rh center with trans-disposed carbonyl and siloxide ligands. The Si...Rh distance (2.8255(4) Å) is sufficiently long that no significant solidstate interaction can be inferred, consistent with the lack of ²⁹Si/¹⁰³Rh coupling by NMR. The loss of a Si/Rh bonding interaction is accompanied by a slight shortening of the Si-OTf bond in **6-OTf** (1.73(2) Å) relative to **1-OTf** (1.796(3) Å). The incorporation of a siloxide within the pincer framework leads to an extraordinarily more acute Si-O-Rh angle (100.2(9)°) compared with other rhodium siloxides (average of 152° for three structurally characterized examples¹²), suggesting a significant degree of strain in the siloxide linkage of 6-OTf and possibly a higher reactivity. The acute Si-O-Rh angle seems to be primarily a consequence of the constraints imposed by the pincer, since Milstein's related complex shows a nearly identical Si-O-Pt angle $(100.5(3)^{\circ})$. 11b

To probe the mechanism of the **1-OTf** \rightarrow **6-OTf** transformation, the effect of added nbd and triflate on the reaction rate was examined. When **1-OTf** was exposed to CO₂ in the presence of added nbd (30 equiv), no reaction was observed, consistent with the expectation that nbd dissociation from the 18-electron complex precedes reaction with CO₂. However, reactions conducted in the presence of excess ["Bu₄N][OTf] or ["Bu₄N][PF₆] (30 equiv) occurred at the identical rates, indicating that the triflate is not outer-sphere during the rate-determining step. Finally, the reaction rate shows a pronounced solvent dependence: the reaction of **1-OTf** with CO₂ in dichloromethane reached 50% conversion to **6-OTf** in <1 h, whereas the same reaction in benzene took 4 h to reach 50% conversion.

Taken together, the above findings point toward interaction of CO_2 with the 14-electron T-shaped [$^{Cy}P_2Si^{OTf}$]Rh intermediate (Scheme 3, Silyl Pathway) or an isomer thereof. Reaction of the triflatosilyl complex would involve anomalous 1,2-insertion of CO_2 into the Rh–Si bond, followed by CO deinsertion (α -siloxide elimination) from the siloxyacyl to afford **6-OTf**. Anomalous insertion of CO_2 into a M–Si bond has been previously proposed 13 but not conclusively demonstrated, and Wolczanski has reported the microscopic reverse of the CO deinsertion step (CO insertion into a Re siloxide). 14

Alternatively, CO₂ could react with [CyP₂Si=]Rh(OTf), the neutral silylene isomer of [CyP₂SiOTf]Rh accessed through Si→Rh triflate migration. In this case, [2+2]-cycloaddition would occur at the Rh=Si unit, followed by cycloreversion and rearrangement to the observed product (Scheme 3, Silylene Pathway). Although [2+2]-cycloaddition of CO₂ to a metal silylene is not known, Grubbs and Hill have described related processes at an iridium carbene¹⁵ and ruthenium carbyne, ¹⁶ respectively, and Banaszak Holl has reported the reversible [2+2]-cycloaddition of CO₂ at a platinum germylene. ¹⁷ Tilley has also studied a net [2+2] of aryl isocyanates at a Ru silylene. ¹⁸

To explore the generality of this unusual reaction and shed further light on the mechanism, several variants of **1-OTf** were tested: base-stabilized silylene complexes **1-DMAP**⁺ and **1-**

 Et_2O^+ and the neutral methylsilyl complex 1-CH₃. 4c,19 The cationic complexes reacted with CO₂ to afford cationic siloxide carbonyl products, 6-DMAP⁺ and 6-Et₂O⁺, that are structurally analogous to 6-OTf. Unlike 6-OTf, complex 6-DMAP+ crystallizes readily and afforded a high-quality structure (Figure 2), lending further support to the formulation of 6-OTf based on NMR and a low-quality structure. As expected based on data for related cobalt silyl/silylene complexes, 4a the 29Si chemical shifts for $6-\text{Et}_2\text{O}^+$ (-26 ppm) and $6-\text{DMAP}^+$ (-34 ppm) are downfield of the neutral 6-OTf (-42 ppm). In spite of their different stabilities (1-DMAP⁺ > 1-OTf > 1-Et₂O⁺) and charges, the DMAP and OTf- complexes react with CO₂ at nearly identical rates. 20 In contrast, the methylsilyl complex 1-CH3 did not react with CO₂ to give 6-CH₃.²¹ The divergent reactivity of 1-CH₃ could support either mechanism, since the methylsilyl complex features both a non-labile Si-C bond (disfavoring the silvlene pathway) and a less electrophilic silicon (disfavoring the anomalous insertion in the silyl pathway).

Scheme 3. Plausible mechanisms for oxygen-atom extrusion from CO_2 by **1-OTf**

Rh/Si Cooperative Scission of CO₂: Computational Elaboration of an Anomalous Insertion Mechanism. With this information in hand, we turned to density functional theory (DFT) calculations to elucidate the intimate mechanism of O-atom abstraction. Calculations were performed with the B97-D3BJ functional and the def2-TZVP basis set, using the SMD solvent model for dichloromethane. This method has been used successfully by Leitner and us to model the reactivity of related rhodium complexes. 9,22

We first set out to discriminate between silvl and silvlene reaction pathways. Experimental studies implicated the need for a labile group on the Si atom (OTf, DMAP, or Et₂O), so our computational studies began with the silvlene pathway (Figure 3). Since nbd dissociation is required for reaction with CO₂, we chose the T-shaped, 14-electron complex [P₂Si^{OTf}]Rh (C-1), formed upon nbd dissociation, as a starting point. Migration of triflate to Rh occurs by an ion pair, such as C-2, leading to silylene complex C-3. We consider ion pair C-2 to be an estimate of the barrier to triflate migration (other configurations of the ion pair are possible), since no concerted triflate migration pathway could be located. Neutral silvlene C-3 undergoes [2+2] cycloaddition with CO₂ with a barrier of about 17 kcal/mol to give a relatively stable cycloadduct C-5. Formation of a rhodium siloxide then occurs in two steps: cleavage of the C-O bond to give CO/silanone complex C-7, followed by formation of the siloxide O-Rh bond to give C-9. This latter complex is high in energy, which could be a consequence of the arrangement of ligands²³ and/or the unusual Rh/silanone bonding interaction (see Supporting Information for an orbital analysis of C-9). The high energy of C-9 means that the barrier to CO₂ splitting by this mechanism is nearly 37 kcal/mol (from C-5), which would be impossible at room temperature. In short, computations predict that silvene complex C-3 is accessible and can react readily

with CO₂ via [2+2]-cycloaddition; however, the silylene pathway is not likely to lead to the observed product **6-OTf** due to the high barrier to form a rhodium siloxide (**TS-8**).

We next turned to direct insertion (silyl pathway), beginning again with T-shaped complex C-1 (Figure 4). Reaction with CO₂ occurs by nucleophilic attack of Rh toward CO₂ to form η^1 -CO₂ complex C-11, which is slightly exergonic. CO₂ binds nearly perpendicular to the plane of the pincer ligand, which is consistent with interaction with the d_{z^2} HOMO of complex C-1 (*vide infra*). Complex C-11 features a relatively strong Rh–CO₂ interaction, based on the short Rh–C bond (2.06 Å) and a decreased O=C=O angle (137°) showing significant rehybridization at carbon. Leitner has computationally studied a number of 5-coordinate Rh(I) η^1 -CO₂ complexes where the O=C=O angle ranges from 133° (for anionic complexes) to nearly 180°; ^{22b} therefore, the structure of C-11 suggests a relatively nucleophilic Rh center.

Unlike the rhodium alkyl complexes reported by Leitner, which undergo normal migratory insertion, C-11 undergoes anomalous insertion of CO₂ via TS-12 with a barrier of about 14 kcal/mol. TS-12 involves an electrophilic attack of silicon on the oxygen of CO₂ to form a 4-membered ring in C-13. Therefore, reaction with CO₂ in the silyl pathway can be described as a stepwise cycloaddition involving nucleophilic attack of Rh, followed by electrophilic attack of Si.

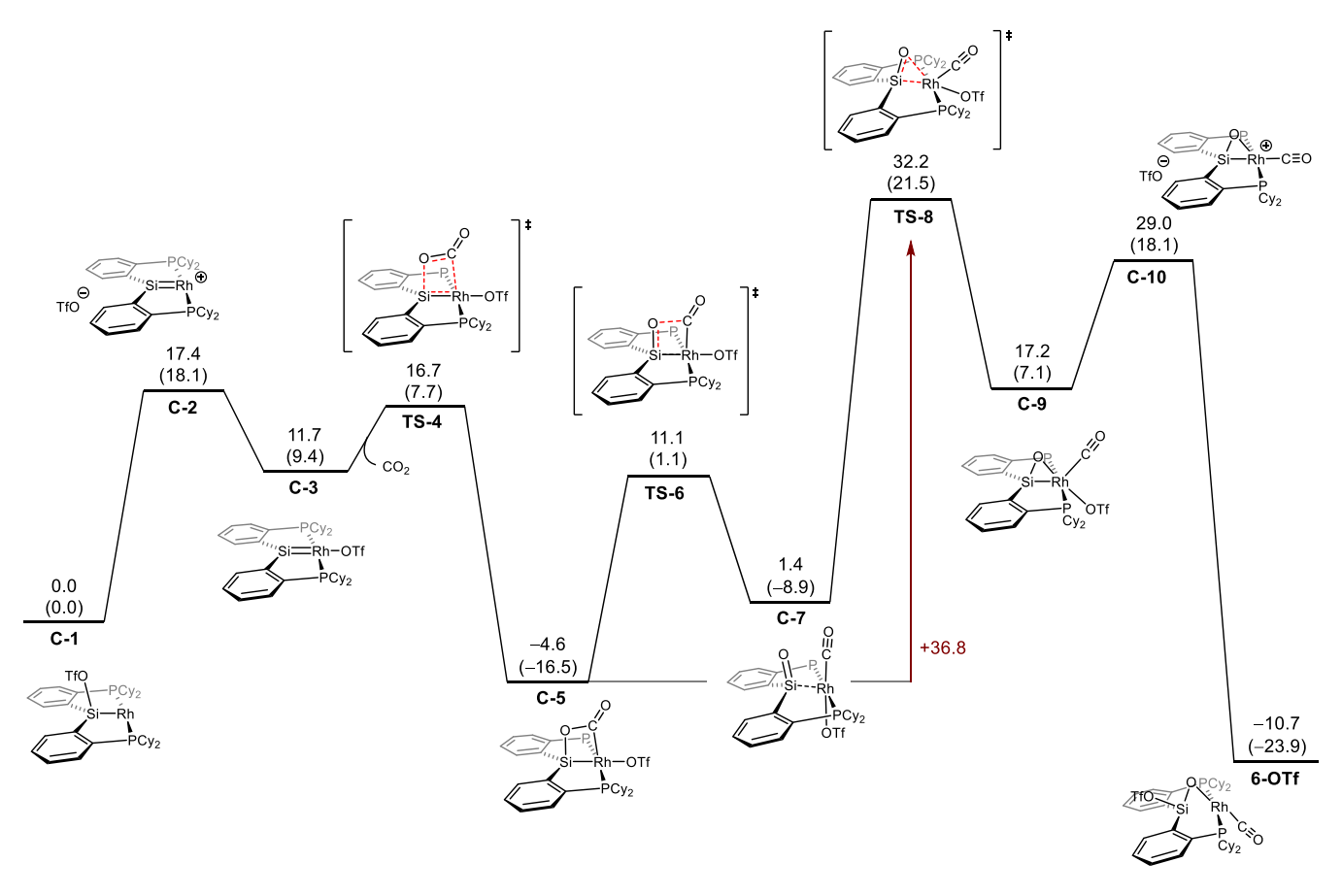


Figure 3. Silylene pathway for cycloaddition of CO₂ with silylene complex C-3 (derived from 1-OTf). Gibbs free energies and enthalpies (in parentheses) in kcal/mol, calculated with B97-D3BJ/def2-TZVP/SMD(dichloromethane).

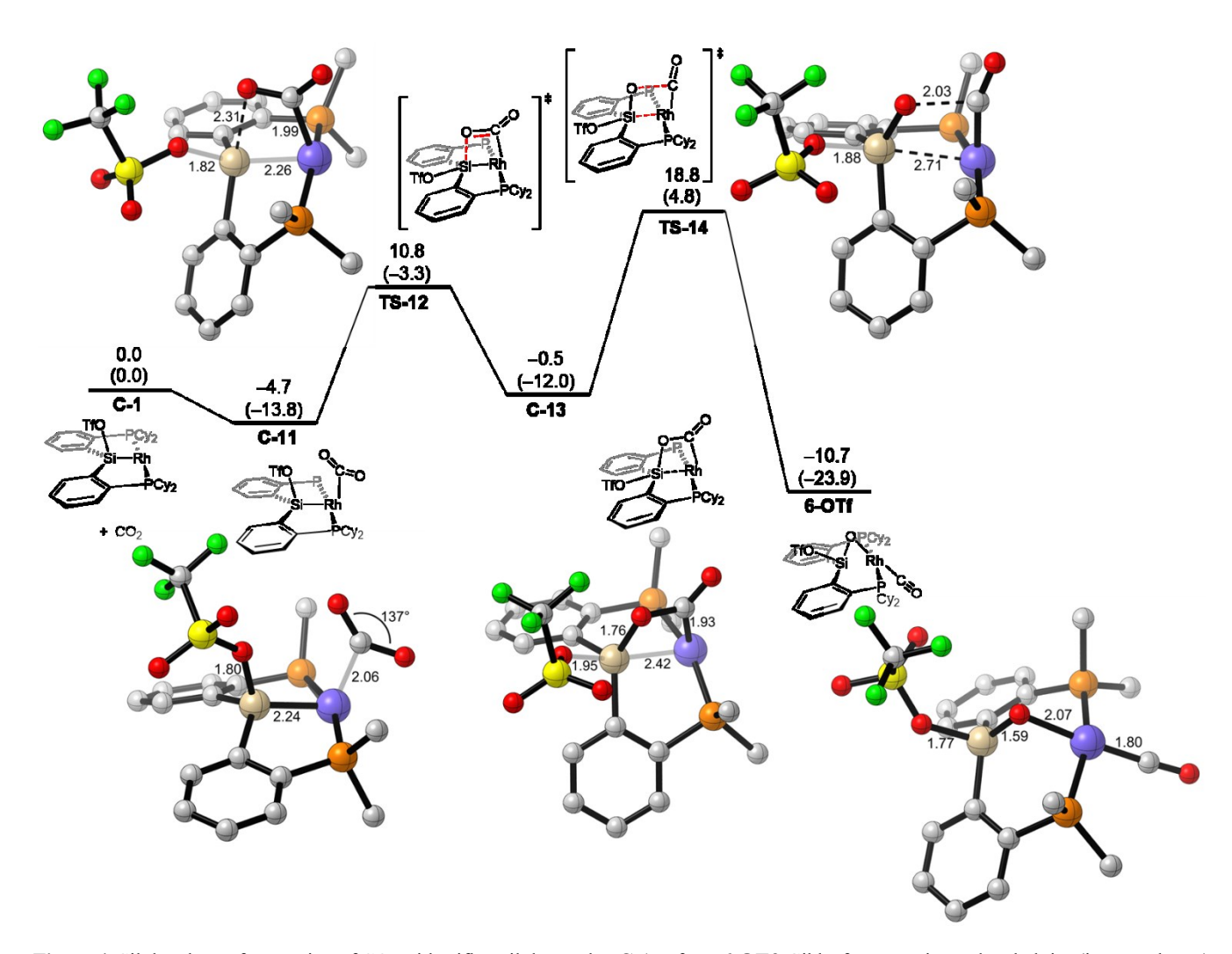


Figure 4. Silyl pathway for reaction of CO₂ with triflatosilyl complex C-1 to form 6-OTf. Gibbs free energies and enthalpies (in parentheses) in kcal/mol, calculated with B97-D3BJ/def2-TZVP/SMD(dichloromethane). Cyclohexyl groups and hydrogen atoms are hidden in 3D structures for clarity.

The structure of C-13 is unusual: the Rh–Si distance has elongated by about 0.2 Å and the Si–OTf distance has elongated by about 0.15 Å compared to C-11. The Si atom is approximately trigonal bipyramidal with apical Rh and OTf groups (sum of equatorial bond angles = 359°). The Rh–Si bond has clearly weakened, but a hypervalent interaction remains. Natural bond orbital (NBO) analysis was used to quantify this change: the NAO Wiberg Bond Index for the Rh–Si bond decreases from 0.77 for C-11 to 0.51 for C-13. Thus, while the formation of C-13 would formally be considered a migratory insertion, the residual Rh/Si interaction suggests that it is similar to a cycloaddition that weakens (but does not break) the Rh–Si bond. Based on computations with an unchelated analogue (vide infra, Figure 5), we believe that the Rh–Si bond in C-13 remains mainly due to chelation in the pincer ligand.

For comparison, we also considered the normal migratory insertion of CO₂ with C-1 to form Si–C and Rh–O bonds. While this process has been observed for nickel and copper silyl complexes, ^{5c,d} for C-1 this migratory insertion is highly disfavored (endergonic by >40 kcal/mol). This finding is consistent with orbital and charge analyses indicating that Rh is the nucleophilic atom in this system (*vide infra*).

Continuing on the reaction pathway, cycloadduct C-13 leads to the observed CO complex 6-OTf in a single step. CO-

deinsertion via **TS-14** is the rate-limiting step with a barrier of about 23 kcal/mol (from **C-11**), consistent with a rapid reaction at room temperature. IRC analysis suggest that CO-deinsertion is an asynchronous process that begins with C–O bond cleavage at **TS-14**. This allows the Si to rehybridize to a tetrahedral geometry, the siloxide to form an O–Rh bond, and the CO ligand to migrate *trans* to the siloxide, all without significant additional barrier (see Supporting Information for details). The formation of **6-OTf** is highly exergonic and the computed structure agrees well with experiment.

Experiments show that the reaction with CO_2 requires a moderately polar solvent (dichloromethane) and the reactivity is greatly decreased in benzene. While this might seem to implicate triflate migration or dissociation (i.e., a silylene pathway), computations show it is instead due to the asynchronous transition state for CO deinsertion (TS-14). Since C–O bond cleavage precedes O–Rh bond formation, a great deal of charge builds up on the siloxide oxygen. A polar solvent is therefore critical to stabilizing this polar transition state (dipole moment for TS-14 = 17.6 D, nearly twice that of C-1 = 10.0 D). Indeed, when the direct insertion pathway is calculated using benzene in place of dichloromethane as the solvent model, the energy of TS-14 increases by about 6 kcal/mol, greatly slowing the overall reaction.

To further understand electronic effects of the silyl group, we studied several derivatives computationally (see the Supporting Information). In general, silyl groups with electron-withdrawing substituents (triflate and DMAP) are more reactive, undergoing CO-deinsertion more rapidly than carbon groups (Me or Ph). This trend is the opposite of what has been reported by Driess for CO₂ cleavage by Cu silyl complexes, where more nucleophilic silyl ligands react more rapidly. However, this difference is expected in light of the different regiochemistries (normal versus anomalous) observed for CO₂ insertion. In the present case, the trend is again explained by the polar, asynchronous nature of **TS-14** and the buildup of negative charge on the siloxide oxygen, which is stabilized by a more electrophilic silyl group.

CO₂ Scission by an Unchelated Rh–Si Complex. To this point, our studies had been motivated by the idea that constrained pincer-type complexes featuring M–Si bonds can promote unusual reactions. However, the findings above imply that unchelated complexes featuring appropriate M–Si bonds might undergo anomalous migratory insertion in the same manner as 1-OTf and its congeners. Thus, we decided to probe whether the pincer ligand was important for reactivity with CO₂.

Surprisingly, the T-shaped triphenylsilyl complex C-15 with simple trimethylphosphine ligands (Figure 5), is predicted by computation to undergo more rapid reaction with CO₂ than C-1, with a rate-limiting barrier (TS-19) of only about 15 kcal/mol (from C-16). While the mechanism of the reaction is the same, the structure of the CO₂ insertion product C-18 is quite different from C-13. Freed from the constraints of chelation, C-18 exhibits no residual Rh–Si interaction (distance of 3.09 Å, NAO Wiberg Bond Index of 0.07) and features a tetrahedral rather than

trigonal bipyramidal silicon center. Furthermore, while a labile group on Si (TfO $^-$, DMAP, or Et₂O) appeared to be important for reactivity of the pincer complex, the unchelated triphenylsilyl complex does not exhibit the same requirement. In addition to providing additional support for an unusual anomalous insertion mechanism of CO₂ into Rh–Si, the calculations on an unchelated complex provide grounds for checking the validity of our computational predictions.

The unchelated complex Ph₃Si-Rh(PMe₃)₃ (7) was prepared by the method of Thorn and Harlow.²⁵ As predicted, exposure of 7 to CO₂ (1 atm) resulted in immediate reaction as judged by ³¹P NMR spectroscopy. Although the product is unstable in the absence of PMe₃, both NMR and IR spectra confirm formation of the siloxide product trans-Ph₃SiO-Rh(PMe)₂(CO) (8, Eq 2). In particular, the ²⁹Si spectrum of 8 shows a significant upfield shift relative to 7 (δ –26.4 ppm for 8 versus 12.2 ppm for 7), with a loss in Rh/Si coupling, and the IR spectrum of 8 exhibits a characteristic carbonyl stretch at 1950 cm⁻¹. Together, these findings confirm that 7 reacts with CO₂ in a fashion analogous to 1-OTf, though much faster, lending further credence to an anomalous insertion mechanism since the Si-Ph bond cleavage to form a silylene is unlikely. The overall process closely resembles the CO2 scission at a rhodium boryl complex described by Kalläne et al.,26 which was proposed to proceed through an insertion pathway but no mechanistic or computational studies were reported.

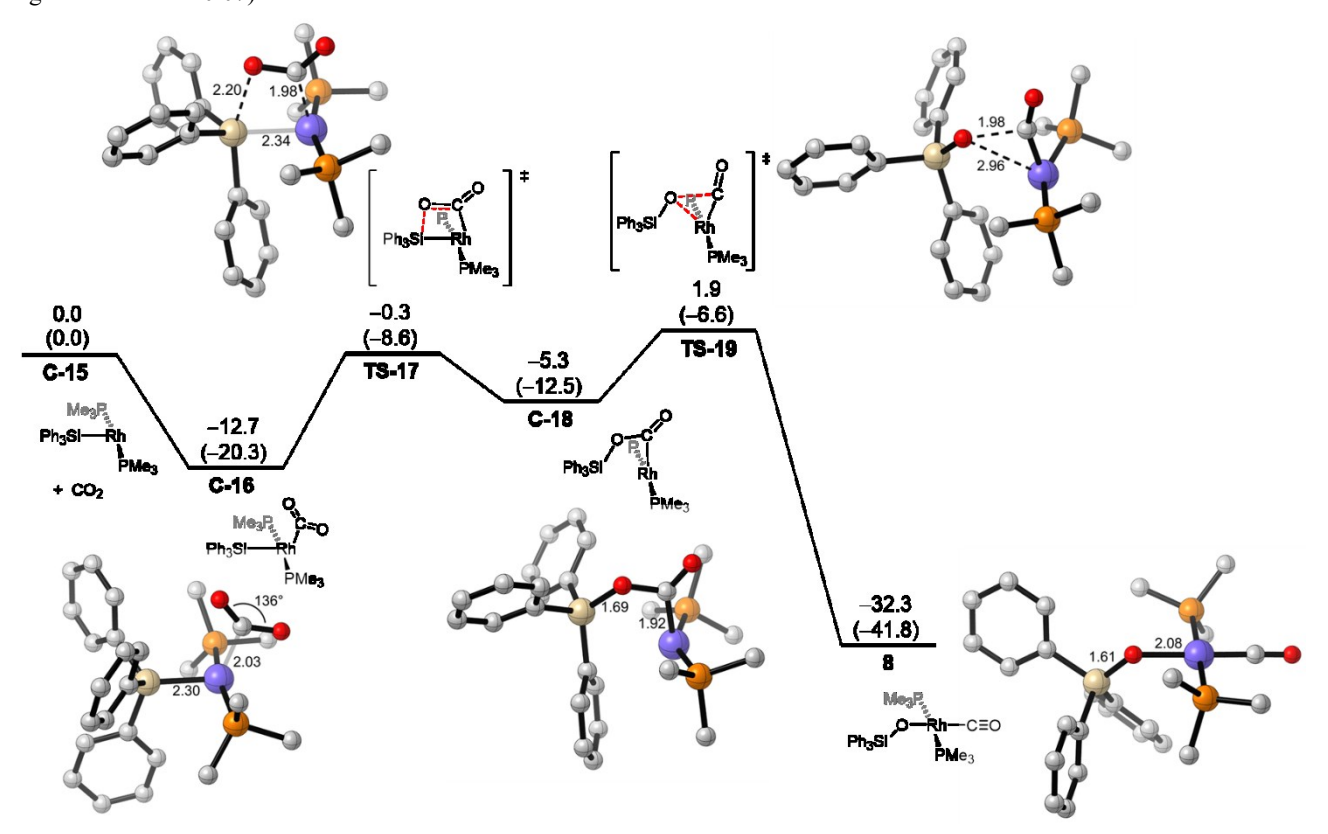


Figure 5. Direct addition of CO₂ with triphenylsilyl complex C-16 (derived from 7) to form 8. Gibbs free energies and enthalpies (in parentheses) in kcal/mol, calculated with B97-D3/def2-TZVP/SMD(dichloromethane). Hydrogen atoms are hidden in 3D structures for clarity.

Factors Controlling the Regiochemistry of CO₂ Insertion.

We next sought to understand the interaction of C-1 with CO₂ in greater detail by examining the molecular orbitals involved. As expected for low-valent rhodium, the HOMO of C-1 is a Rhcentered d_{z^2} orbital (Table 1), which will interact favorably with LUMO of CO₂ to form adduct C-11. The metal-centered HOMO supports the description of this interaction as a stepwise cycloaddition rather than migratory insertion, which would involve the Rh–Si σ bond.²⁷ Further evidence for the nucleophilicity of Rh and electrophilicity of Si in complex C-1 is found by examining natural population analysis (NPA) charges: -0.62 on Rh and +1.56 on Si. Unchelated complex C-15 has an even more negatively charged Rh center, in line with the greater reactivity of Ph₃Si-Rh(PMe₃)₃ (7). We also calculated the total charge on the silyl group, as computed in previous studies of silyl complex reactivity;^{27a} however, we found this parameter to have little correlation to the observed reactivity in our system.

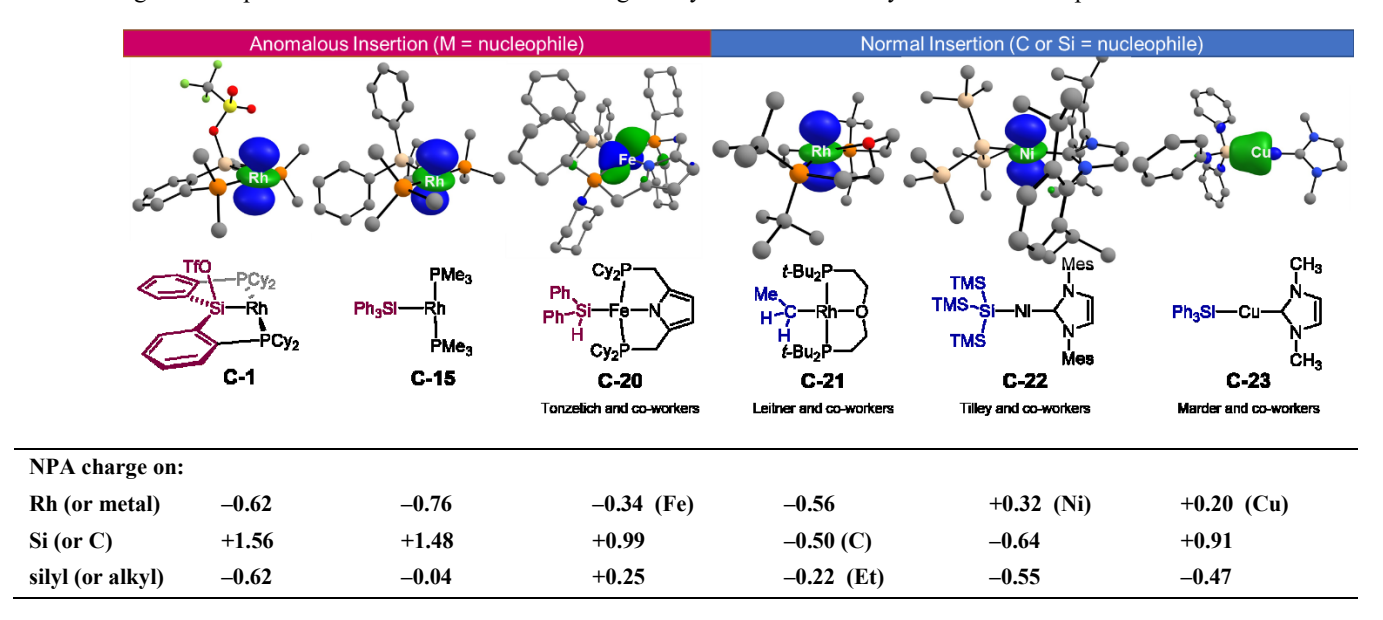
Seeking to generalize the factors that control regiochemistry of CO₂ insertion, we computed the HOMO and NPA charges for several related complexes. Tonzetich and co-workers very recently reported an Fe(II) silyl complex (C-20) capable of reducing CO₂ to form an Fe(CO) complex.¹³ Though the detailed mechanism has not been fully explored, it is postulated to involve anomalous insertion of CO₂ to form a siloxyacyl complex analogous to C-18. In line with our Rh complexes, we find C-20 has NPA charges of -0.34 on Fe and +0.99 on Si.

Next, we considered several complexes reported to undergo normal migratory insertion of CO₂, where a silyl or alkyl ligand attacks the carbon of CO₂. Leitner has studied several alkylrhodium complexes, such as C-21, and found that more negative NPA charge on carbon led to lower computed barrier for migratory insertion. ^{22b} Our calculations are in line with that trend, though it is worth noting that in C-21 Rh also bears a negative charge of similar magnitude to that of C. Similarly, Ni^{5d} and Cu^{5c} silyl complexes C-22 and C-23 have been demonstrated by Tilley and Marder, respectively, to undergo normal migratory insertion of CO₂. In the case of Ni complex C-22, the regioselectivity is well rationalized by a negative charge on Si. However, Cu complex C-23, which bears a positive NPA charge on Si, appears to be an outlier. As Yates has previously noted, summing the charges on the entire Ph₃Si ligand of C-23 gives a negative charge, in line with a nucleophilic silyl group. ^{27a}

Bearing in mind the importance of frontier orbitals in governing the reactivity of C-1 (Figure 6), we also calculated the HOMO of each complex (shown in Table 1). In all cases but Cu complex C-23, the HOMO is a metal-centered d-orbital. In C-23 the HOMO is a Cu–Si σ -bonding orbital, which is consistent with a normal migratory insertion and may account for its apparent outlier status when charge distributions alone are considered.

Taken together, simple charge and orbital analyses can lend insight into the reactivity of each complex, but no single property can describe the reactivity completely. For complexes in which the HOMO is metal-centered, one can use the charge on the Si (or C) atom to predict whether the silyl (or alkyl) is nucleophilic. Nevertheless, exceptions may exist and caution must be used in predicting reactivity from computed properties, which are no substitute for experimental studies.

Table 1. Highest-occupied molecular orbital and NPA charge analysis for rhodium silyl and related complexes.



Reactivity of the CO₂ Scission Product. A preliminary reactivity study of 6-OTf shows that the siloxide unit obtained via oxygen-atom transfer from CO₂ is amenable to further elaboration. Unlike 1-OTf, complex 6-OTf is quite sensitive to water, giving complex 9-OTf with an unusual Rh-coordinated silanol (Scheme 4). The most closely related example is a (PSi^{OH}P)Ir complex reported by Sola and co-workers that was obtained by hydrolysis of an Ir–Si bond.²⁸ Ozerov has also reported Pd pincer complexes with coordinating silanols.²⁹ In the solid state, 9-

OTf shows two-point hydrogen bonding with the triflate counterion (Figure 6), and its moderate solubility in benzene suggests that a strong interaction is maintained in nonpolar solvents. The O \underline{H} chemical shifts show a substantial solvent dependence (δ 10.93 and 6.78 ppm in C_6D_6 versus δ 9.35 and 5.60 ppm in CD_2Cl_2), suggesting that the triflate may not be closely associated in polar solvents.

Scheme 4.

A solid-state structure of **9-OTf** was obtained (Figure 6), showing several points of distinction relative to the siloxide product **6-OTf** from which it is prepared. Most importantly, the Si–O–Rh bond angle is relieved (107.7(1)° for **9-OTf** versus 100.2(9)° for **6-OTf**), leading to a considerably longer Si···Rh distance (3.0264(9) Å for **9-OTf** versus 2.8255(4) Å for **6-OTf**). We have observed that **9-OTf** decomposes under vacuum, but clean reactivity has not yet been observed.

The acute Si–O–Rh bond in **6-OTf**, combined with the expected low Rh–O bond strength, suggests that Rh–O bond cleavage may be effected with appropriate reagents. By analogy with Sadighi and Marder's use of diborane and silylborane reagents to cleave Cu–OBR₂ and Cu–OSiR₃, we found that **6-OTf** reacts cleanly with pinacolborane (HBpin), forming a new B–O bond, cleaving the O–Rh bond, and reforming the Si–Rh linkage with migration of triflate to rhodium to afford **10-OTf** (Scheme 4 and Figure 6). This reaction closely resembles Driess's reported hydroboration of a Ni–O bond in a nickel-bound silanone.³⁰ To this point, further reactions to liberate oxygenated product by cleaving the Si–O bond have been unsuccessful, likely due to the high Si–O bond strength.

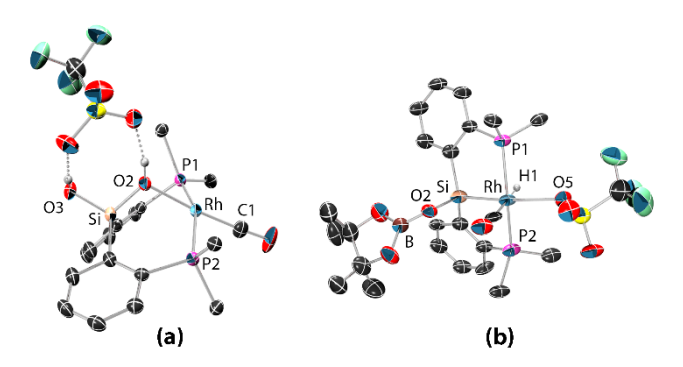


Figure 6. Molecular representations of (a) **9-OTf** and (b) **10-OTf** with thermal ellipsoids at 50% probability. Most hydrogen atoms have been removed and phosphine substituents are truncated for clarity. Selected bond lengths (Å) and angles (deg) for **9-OTf**: Rh–C1, 1.793(3); Rh–O2, 2.092(2); Si–O2, 1.641(2); O2–Rh–C1, 175.28(13); P1–Rh–P2, 158.38(3); Si–O2–Rh, 107.72(10). For **10-OTf**: Rh–Si, 2.2718(19); Rh–C1, 1.936(9); Rh–O5, 2.336(4); Rh–H, 1.29(4); Si–Rh–H1, 83.6(18); Si–Rh–O5, 165.90(12); P1–Rh–P2, 156.82(6).

DISCUSSION

The anomalous 1,2-insertion of CO_2 is an unusual pathway, occasionally observed for M–H bonds³¹ but not conclusively demonstrated for M–Si bonds due to the kinetic nucleophilicity of the silyl unit that can dominate over silicon's thermodynamic oxophilicity. ^{5c,24,27a} This closely resembles the situation encountered with metal boryls, ³² which have been examined in the context of CO_2 activation. ^{27b,33} Even in cases such as the (NHC)Cu–E systems examined by Sadighi and Marder (E = BR₂, SiR₃), which give nearly identical overall transformations to those presented here, the mechanism involves a normal insertion of CO_2 followed by 1,2-boryl or –silyl migration to form the B–O or Si–O bond. ^{5c,27b,33}

The present system has been tuned such that silicon acts as a kinetic electrophile during the insertion reaction. This pathway is supported by the electron-rich, d^8 rhodium center, and the relatively electrophilic silicon center working in concert. The fact that the more electron-rich methylsilyl complex **1-Me** does not react in the same way as **1-OTf**, **1-DMAP**⁺, and **1-Et₂O**⁺ provides strong support for the notion that a sufficiently electron-poor silicon center is required in order for the reaction to take place. Computations support a $Si^{\delta+}$ -Rh $^{\delta-}$ polarization and suggest that replacement of Si with C would reverse the polarization sufficiently to favor a normal insertion of CO_2 . By comparison with copper boryl and silyl work from Sadighi and Marder (where normal insertion is implicated), the metal is more electron-rich and the silicon more electron-poor.

The anomalous insertion pathway presented here provides a more efficient route to CO_2 deoxygenation than normal-insertion routes that give the same net reaction, since CO deinsertion should be a lower-barrier process than 1,2-silyl migration. This is borne out in the reactions described, for which overall barriers are low and no intermediates are observable; in fact, the unchelated version reacts instantly with CO_2 . In contrast, the (NHC)Cu–SiR3 complexes described by Marder afford observable (NHC)Cu–OC(O)SiR3 intermediates that slowly convert to the siloxide products. 5c

Far from being unexpected, the anomalous insertion of CO₂ is likely to be favored in general for properly tuned metal silyl complexes with $Si^{\delta+}$ - $M^{\delta-}$ polarization, particularly those with electron-rich, unsaturated metals. In fact, our findings suggest that the most closely related transformations from the literature (deoxygenation of CO₂ by a rhodium boryl and desulfurization of COS by a rhodium germyl)^{26,34} probably occur by a similar anomalous insertion route, though no mechanistic details were provided in the original manuscripts. Such a pathway has also been proposed by Tonzetich for stoichiometric CO2 reduction by an iron(II) silyl complex¹³ based on observation of an Ojimatype^{7b} 2,1-insertion of benzaldehydes, though thorough mechanistic studies were not conducted. These proposals are consistent with computations by Yates and co-workers predicting that palladium silyl, germyl, and stannyl complexes featuring phosphine and alkyl co-ligands should undergo anomalous insertion of CO₂.^{27a} Furthermore, we propose that anomalous insertion into M-C bonds may be promoted by strategic integration of electron-withdrawing groups at carbon and choice of an electronegative metal with electron-donating supporting lig-

Comparison with the related cleavage of CO_2 at a Zr/Co heterobimetallic complex reported by Thomas also proves illuminating.³⁵ In fact, both the structure of Thomas' μ -oxo product and its subsequent reactivity (cleavage of the Co–O bond by

silane to afford a zirconium siloxide) closely resemble the transformations reported here. The close analogy highlights the possible similarities between M–M and M–Si bonds.

We have not yet been able to develop the pathway presented in this manuscript into a catalytic reaction. Although the CO_2 cleavage product **6-OTf** is reactive, the Si–O bond is quite strong. We have not yet seen evidence for Si–O cleavage, even with strong reductants, though we are continuing to pursue this avenue. More promisingly, the findings presented here suggest that similar pathways may be accessible for elements with more labile bonds to oxygen, allowing O-atom transfer from CO_2 cleavage products.

CONCLUSIONS

In conclusion, this work has shown that CO_2 can be activated and reduced at polarized $Rh^{\delta-}$ – $Si^{\delta+}$ bonds via anomalous insertion to give a siloxyacyl intermediate, followed by CO deinsertion. Although previous examples of CO_2 insertion into M–Si bonds exhibited a normal insertion mode (forming M–O, and C–Si bonds), we see no evidence for the normal process and instead calculate it to be a prohibitively high-energy pathway. Although the net process closely resembles CO_2 deoxygenation at (NHC)Cu–SiR₃ complexes previously reported by Marder, ^{5c} the fact that a 1,2-silyl migration is not required here leads to much lower barriers for the reaction (allowing the unchelated complex to react instantly at ambient temperature, compared with 22 h for the (NHC)Cu system).

For both chelated and unchelated P2Rh-SiR3 complexes, interaction with CO₂ appears to be initiated by a nucleophilic and coordinatively unsaturated Rh center rather than by a nucleophilic Rh-X σ bond. The "anomalous" regiochemistry of the insertion process is a predictable consequence of the polarized Rh^{δ} -Si^{δ +} façade. This finding suggests that silicon lies right on the line dividing preference for normal and anomalous insertion pathways, so the regiochemistry of CO₂ insertion can be controlled by tuning related systems. We expect that the more electronegative late metals (Ru, Os, Rh, Ir, Pd, Pt) may all exhibit a similar anomalous insertion process with CO₂, including at other metal/main-group σ bonds (e.g., boryl, germyl, and phosphide complexes). This notion is supported by the recent report of CO₂ splitting in a similar fashion to that reported here at the Fe-P bond of an iron(0) phosphinine complex.³⁶ In general, this work has demonstrated how the electronic façade of a metal/main-group unit impacts the selectivity of insertion reactions. Further explorations will be focused on understanding the generality of these findings and extending them to catalytically useful systems.

EXPERIMENTAL SECTION

General Considerations. All manipulations were carried out in a nitrogen-filled glove box. Routine solvents were purchased from commercial suppliers and were deoxygenated and dried using a Glass Contour Solvent Purification System and were stored over 4-Å molecular sieves in an inert-atmosphere glove box. Benzene and pentane were purchased in anhydrous and oxygen-free form from Aldrich and used as received. Fluorobenzene was dried via reflux over CaH₂, vacuum-transferred, and stored over 4-Å molecular sieves. 1-OTf^{4c} and 1-CH₃¹⁹ were prepared according to published methods. NMR solvents were vacuum transferred from sodium/benzophenone (benzene-*d*₆) or heated to reflux over calcium hydride and vacuum transferred (dichloromethane-*d*₂), then stored in a nitrogen-filled glove box

prior to use. Other reagents were purchased from commercial vendors and used without further purification.

Characterization Methods. NMR spectra were recorded at ambient temperature on a Bruker Avance III HD 400 High Performance Digital NMR spectrometer. ¹H and ¹³C NMR chemical shifts were referenced to residual solvent; ¹⁹F, ²⁹Si, and ³¹P NMR chemical shifts are reported relative to external standards of neat trifluoroacetic acid (–78.55 ppm), tetramethylsilane (0 ppm), and 85% H₃PO₄ (0 ppm), respectively. IR spectra were recorded on a Thermo Scientific Nicolet iS5 FTIR spectrometer using a solution IR cell with NaCl windows. Microanalysis was carried out by Midwest Microlab, LLC.

Computational Methods. DFT calculations were performed with Gaussian 09.³⁷ Computed structures are illustrated using CYLView, ³⁸ and molecular orbitals are rendered with Chem-Craft. ³⁹ Calculations were performed with the B97-D3⁴⁰ functional and the def2-TZVP basis set, using the SMD solvent model for dichloromethane. Density fitting was enabled using the W06 fitting set, which is designed for use with the def2-TZVP basis set. ⁴¹ Thermal corrections were calculated from unscaled vibrational frequencies at the same level of theory using a standard state of room temperature (298 K) and 1 mol/L. The nature of transition states was verified by the presence of a single imaginary frequency. IRC calculations were performed to verify the transition state connected to the appropriate intermediates.

 $[(^{Cy}P_2Si^{DMAP})Rh(nbd)][OTf]$ ([1-DMAP][OTf]). Complex 1-OTf (131.2 mg, 0.143 mmol) and norbornadiene (ca. 15 μL) were dissolved in benzene (2 mL) in a 20-mL scintillation vial. 4-(Dimethylamino)pyridine (18 mg, 0.15 mmol) was dissolved in benzene (2 mL) and added to the solution of 1-OTf with stirring, causing a precipitate to form. After 30 min, pentane (5 mL) was added and undissolved solids were collected by filtration, redissolved in dichloromethane (2 mL), filtered, and concentrated in vacuo to afford [1-DMAP][OTf] as a light yellow powder. Yield: 126.3 mg (85%). ¹H NMR (CD₂Cl₂, 400 MHz): δ 7.78 (d, J = 7.3 Hz, 2H), 7.48 (dd, $J_1 = 7.2$ Hz, $J_2 = 1.1$ Hz, 2H), 7.45-7.35 (m, 6H), 6.59 (d, J = 7.8 Hz, 2H), 5.34 (s, 2H), 3.42 (s, 2H), 3.17 (s, 6H, $-N(CH_3)_2$), 2.79 (t, 11.4 Hz, 2H), 2.40(s, 2H), 2.20–2.06 (m, 4H), 1.97–1.69 (m, 12H), 1.69–1.55 (m, 6H), 1.55–1.02 (m, 20H), 0.91 (q, J = 12.1 Hz, 2H). ${}^{13}C\{{}^{1}H\}$ NMR (CD₂Cl₂, 101 MHz): δ 156.7, 150.7–150.0 (m), 148.4– 147.9 (m), 144.3, 132.5 (t, J = 10 Hz), 130.2, 130.1, 129.9, 128.8, 121.6 (q, J = 322 Hz, CF_3), 76.2, 64.5, 48.1, 42.9 (t, J =11 Hz), 39.0 (t, J = 3.7 Hz), 34.2–33.1 (m), 31.2, 30.2, 29.6, 29.5, 28.3 (t, J = 4.4 Hz), 28.2 (t, J = 5.5 Hz), 27.8 (t, J = 5.3, Hz), 27.6 (t, J = 5.1 Hz), 27.2, 26.4. ¹⁹F{¹H} NMR (CD₂Cl₂, 376 MHz): δ-78.9. ²⁹Si{¹H} NMR (CD₂Cl₂, 80 MHz): δ 86.0 (dt, ${}^{1}J_{RhSi} = 46 \text{ Hz}$, ${}^{2}J_{PSi} = 17 \text{ Hz}$). ${}^{31}P\{{}^{1}H\}$ NMR (C₆D₆, 162 MHz): δ 57.8 (${}^{1}J_{PRh} = 134 \text{ Hz}$). Anal. calcd. for C₅₁H₇₀F₃N₂O₃P₂RhSSi: C, 58.84; H, 6.78; N, 2.69. Found: C, 58.65; H, 6.89; N, 2.50.

$(^{Cy}P_2Si^{O2CH})Rh(H)(OTf)$ (3-OTf).

Method A: Complex **1-OTf** (31.3 mg, 0.0341 mmol) was dissolved in dichloromethane (ca. 4 mL) in a 20-mL scintillation vial, and a stock solution of formic acid in benzene (0.28 mL, 141.3 mM, 0.040 mmol) was added via syringe, causing an immediate lightening of the solution to pale yellow. After 30 min, volatiles were removed *in vacuo* to form a yellow film that was redissolved in diethyl ether (2 mL) and recrystallized at – 35°C to afford analytically pure **3-OTf** as a mixture (96:4) of isomers; due to overlapping signals, only selected NMR data

are presented for the minor isomer. Yield: 23.1 mg (78%). Ma**jor Isomer**: ¹H NMR (C₆D₆, 400 MHz): δ 8.65 (d, J = 7.4 Hz, 2H), 7.68 (s, 1H, O_2CH), 7.30 (dt, $J_1 = 6.4$ Hz, $J_2 = 2.8$ Hz, 2H), 7.23 (tq, $J_1 = 7.4$ Hz, $J_2 = 1.1$ Hz, 2H), 7.08 (tq, $J_1 = 7.6$ Hz, J_2 = 1.1 Hz, 2H), 2.99 (t, J = 12.0 Hz, 2H), 2.59 (d, J = 13.3 Hz, 2H), 2.49-2.38 (m, 2H), 2.27 (d, J = 13.5 Hz, 2H), 2.19-2.04(m, 2H), 1.89 (d, J = 12.1 Hz, 2H), 1.81 (d, J = 10.2 Hz, 2H),1.72-1.56 (m, 8H), 1.50 (d, J = 12.8 Hz, 4H), 1.39-1.01 (m, 14H), 0.91–0.64 (m, 4H), -23.00 (dt, ${}^{1}J_{RhH} = 32.7$ Hz, ${}^{2}J_{PH} =$ 13.2 Hz, 1H). ${}^{13}C\{{}^{1}H\}$ NMR (C₆D₆, 101 MHz): δ 159.7 (d, J =28 Hz), 151.1 (td, $J_1 = 22$ Hz, $J_2 = 5.0$ Hz), 141.3 (td, $J_1 = 23$ Hz, $J_2 = 3.9$ Hz), 135.4–134.8 (m), 131.1–128.5 (m), 34.4 (m), 33.7 (dt, $J_1 = 19$ Hz, $J_2 = 9.7$ Hz), 31.0, 29.3, 28.9, 27.3, 27.0, 26.3. $^{19}F\{^{1}H\}$ NMR (C₆D₆, 376 MHz): δ -77.6. $^{29}Si\{^{1}H\}$ NMR $(C_6D_6, 80 \text{ MHz})$: δ 48.3 (dt, ${}^1J_{RhSi} = 42.1 \text{ Hz}, {}^2J_{PSi} = 5.2 \text{ Hz}$). ³¹P{¹H} NMR (C₆D₆, 162 MHz): δ 59.4 (¹ J_{PRh} = 116 Hz). IR (CH₂Cl₂, cm⁻¹): v 1697 (formate C=O). **Minor Isomer**: ¹H NMR (C₆D₆, 400 MHz): δ –19.44 (dt, ${}^{1}J_{RhH}$ = 28.3 Hz, ${}^{2}J_{PH}$ = 12.4 Hz, 1H). ${}^{31}P\{{}^{1}H\}$ NMR (C₆D₆, 162 MHz): δ 59.8 (d, ${}^{1}J_{PRh}$ = 114 Hz). Anal. calcd. for C₃₈H₅₄F₃O₅P₂RhSSi: C, 52.29; H, 6.24. Found: C, 51.99; H, 6.53.

Method B: Complex **2-OTf** was prepared as previously described^{4c} from **1-OTf** (10 mg, 0.011 mmol) in diethyl ether (0.75 mL) in a J Young NMR tube. The reaction was monitored by ³¹P NMR spectroscopy to ensure complete conversion to **2-OTf**. The resulting solution was subjected to one freeze–pump—thaw degas cycle and placed under CO₂ (1 atm). After 90 min, the formation of **3-OTf** in 78% yield (with the remaining product being primarily **4-OTf**) was noted by ³¹P NMR spectroscopy.

 $(^{\text{Cy}}\text{P}_2\text{Si}^{\text{Me}})\text{Rh}(\text{H})(\kappa^2\text{-CO}_2\text{H})$ (5-CH₃). Complex 1-CH₃ (ca. 20 mg) was dissolved in benzene (0.75 mL) and transferred to a J Young NMR tube. The sample was subjected to one freezepump—that cycle and the atmosphere backfilled with H₂ (1 atm), causing the solution to darken considerably then lighten as the H₂ adduct formed, as reported previously. After complete conversion to (CyP₂Si^{Me})Rh(H₂) (4-CH₃) was confirmed by ³¹P NMR spectroscopy (δ 74.3 (br d, ${}^{1}J_{RhP} = 128$ Hz)), the solution was subjected to another freeze-pump-thaw cycle and the headspace replaced with CO₂ (1 atm). Complete conversion to formate complex 5-CH₃ occurred within 10 min. Although 5-CH₃ was not isolated in pure form, its identity was confirmed by comparison to the closely related hydrido formate complex reported by Milstein^{8a} and its purity was >99%, as judged by ³¹P and ¹H NMR spectroscopies. ¹H NMR (C₆D₆, 400 MHz): δ 8.87 (s, 1H, O₂CH), 8.02 (dd, $J_1 = 7.4$ Hz, $J_2 = 1.5$ Hz, 2H), 7.45– 7.40 (m, 2H), 7.26 (tq, $J_1 = 7.3$ Hz, $J_2 = 1.2$ Hz, 2H), 7.18–7.13 (m overlapping with C₆HD₅, 2H), 2.54 (d, 12.2 Hz, 2H), 2.39 (apparent q, J = 11.5 Hz, 2H), 2.28 (t, J = 12.4 Hz, 4H), 2.12– 2.06 (m, 2H), 1.91–1.81 (m, 4H), 1.72–1.61 (m, 6H), 1.60–1.46 (m, 8H), 1.39-1.17 (m, 10H), 1.09-0.90 (m, 6H), 0.88 (s, 3H, Si-CH₃), -21.22 (dt, ${}^{1}J_{RhH} = 25.0$ Hz, ${}^{2}J_{PH} = 14.8$ Hz, 1H, Rh-H). 13 C $\{^{1}$ H $\}$ NMR (C₆D₆, 101 MHz): δ 170.1 (CO₂H), 157.9 $(td, J_1 = 24 Hz, J_2 = 4.1 Hz), 141.6 (td, J_1 = 23 Hz, J_2 = 4.7 Hz),$ 131.9 (t, J = 10 Hz), 130.0, 129.1, 124.4, 38.3, 36.4, 35.6 (t, J =13 Hz), 35.5 (t, J = 9.0 Hz), 30.0, 29.7, 29.3, 28.8, 27.5, 27.4– 27.0 (m), 26.7, 26.1, 6.2 (Si– CH_3). $^{29}Si\{^1H\}$ NMR (C_6D_6 , 80 MHz): δ 48.7 (dt, ${}^{1}J_{\text{RhSi}} = 33$ Hz, ${}^{2}J_{\text{PSi}} = 5.0$ Hz). ${}^{31}P\{{}^{1}H\}$ NMR $(C_6D_6, 162 \text{ MHz})$: $\delta 61.8 \text{ (d, }^1J_{RhP} = 120 \text{ Hz})$.

[^{Cy}P₂Si^{(OTf)(µ-O)}]Rh(CO) (6-OTf). Complex 1-OTf (140.0 mg, 0.152 mmol) was dissolved in dichloromethane (5 mL) and

transferred to a 25-mL Schlenk-style pressure tube. The solution was subjected to one freeze-pump-thaw cycle and the headspace was backfilled with CO₂ (1 atm). The reaction was allowed to proceed with stirring for 2.5 h at ambient temperature. Volatiles were removed in vacuo to afford a yellow film, which as redissolved and crystallized from a minimal volume of 4:1 diethyl ether/dichloromethane to afford pure 6-OTf. Single crystals suitable for X-ray diffraction were obtained by slow cross-diffusion of dichloromethane/hexane at -35 °C. Yield: 42.2 mg (32%). ¹H NMR (CD₂Cl₂, 400 MHz): δ 8.05–7.98 (m, 2H), 7.51–7.43 (m, 6H), 2.62–2.52 (m, 2H), 2.51–2.41 (m, 2H), 2.30 (d, J = 12.8 Hz, 2H), 2.05 (d, J = 12.9 Hz, 2H), 4.05 (m,4H), 1.81–1.13 (m, 32H). 13 C $\{^{1}$ H $\}$ NMR (CD $_{2}$ Cl $_{2}$, 101 MHz): δ 194.2 (dt, ${}^{1}J_{RhC} = 72 \text{ Hz}$, ${}^{2}J_{PC} = 13 \text{ Hz}$, Rh–CO), 143.8 (t, J =9.5 Hz), 139.4 (t, J = 17 Hz), 136.3 (t, J = 5.9 Hz), 131.4, 130.3 $(t, J = 3.0 \text{ Hz}), 129.5, 119.1 (q, {}^{1}J_{CF} = 319 \text{ Hz}, CF_{3}), 37.9 (t, J = 3.0 \text{ Hz})$ 11 Hz), 32.9, 32.6 (td, $J_1 = 12$ Hz, $J_2 = 2.1$ Hz), 28.5–28.2 (m), 28.0–27.8 (m), 27.5, 27.2 (dt, $J_1 = 12$ Hz, $J_2 = 6.0$ Hz), 26.9, 26.3. $^{19}F\{^{1}H\}$ NMR (C₆D₆, 376 MHz): δ –77.1. $^{29}Si\{^{1}H\}$ NMR $(C_6D_6, 80 \text{ MHz}): \delta -42.1 \text{ (t, }^3J_{PSi} = 7.5 \text{ Hz}). \, ^{31}P\{^1H\} \text{ NMR}$ $(C_6D_6, 162 \text{ MHz}): \delta 39.6 (^1J_{PRh} = 125 \text{ Hz}). \text{ IR } (CH_2Cl_2, \text{cm}^{-1}): v$ 1955 (CO). NOTE: The product was quite hydrolytically sensitive and unstable to extended storage at ambient temperature, so suitable microanalysis was not obtained.

 $\hspace{1cm} \hspace{1cm} \hspace{1cm}$ plex [1-DMAP][OTf] (25.3 mg, 0.0243 mmol) was dissolved in dichloromethane (3 mL) and transferred to a 25-mL Schlenkstyle pressure tube. The solution was subjected to one freezepump-thaw cycle and the headspace was backfilled with CO₂ (1 atm). The reaction was allowed to proceed with stirring for 2.5 h at ambient temperature, then volatiles were removed in vacuo to afford a yellow powder. Single crystals of [6-DMAP||OTf| suitable for X-ray analysis was obtained by benzene/hexamethyldisiloxane vapor diffusion at ambient temperature. Crystallized yield: 18.4 mg (76%). ¹H NMR (CD₂Cl₂, 400 MHz): δ 7.78 (d, J = 7.4 Hz, 2H), 7.68–7.62 (m, 2H), 7.59 (t, J $= 7.4 \text{ Hz}, 2\text{H}, 7.54 - 7.48 \text{ (m, 4H)}, 3.19 \text{ (s, 6H, -N(C}H_3)_2), 2.60$ (t, J = 10.6 Hz, 2H), 2.32-2.13 (m, 4H), 2.04 (t, J = 11.1 Hz,4H), 1.91 (d, J = 11.8 Hz, 2H), 1.82 (d, J = 8.9 Hz, 2H), 1.78– 1.68 (br m, 6H), 1.68–1.52 (m, 10H), 1.52–1.42 (m, 4H), 1.42– 1.26 (m, 4H), 1.26–1.10 (m, 8H). ¹³C{¹H} NMR (CD₂Cl₂, 101 MHz): δ 157.4, 144.1, 141.5 (t, J = 9.3 Hz), 140.5 (t, J = 16.5Hz), 136.5 (t, J = 5.8 Hz), 132.6, 131.2 (t, J = 2.8 Hz), 129.8, 108.1, 40.6, 38.4 (t, J = 10 Hz), 33.7 (t, J = 12 Hz), 32.6, 28.6, 28.4 (t, J = 6.8 Hz), 28.3, 27.9 (t, J = 5.2 Hz), 27.1 (dt, J = 13Hz, J = 6.1 Hz), 26.7, 26.2. ¹⁹F{¹H} NMR (CD₂Cl₂, 376 MHz): δ -78.9. ²⁹Si{¹H} NMR (CD₂Cl₂, 80 MHz): δ -34.0 (t, ³ J_{PSi} = 6.9 Hz). ${}^{31}P\{{}^{1}H\}$ NMR (CD₂Cl₂, 162 MHz): δ 38.7 (${}^{1}J_{PRh}$ = 127 Hz). IR (CH₂Cl₂, cm⁻¹): v 1948 (CO). Anal. calcd. for C₄₅H₆₂F₃N₂O₅P₂RhSSi: C, 54.43; H, 6.29; N, 2.82. Found: C, 54.67; H, 6.33; N, 2.89.

$[({^{Cy}P_2Si^{(Et2O)(\mu-O)}})Rh(CO)][B(C_6F_5)_4]\ ([6-Et_2O][BArF]). \\$

Method A. Complex **4-OTf** (22.7 mg, 0.026 mmol) was dissolved in dichloromethane (1 mL), and a solution of LiB(C₆F₅)₄·2.5Et₂O (22 mg, 0.026 mmol) in dichloromethane (2 mL) was added to it with stirring. The reaction was allowed to proceed 1 h, and all volatiles were removed *in vacuo* to give a yellow oil. The oil was extracted into benzene (2 mL) and filtered to remove LiOTf, then lyophilized to afford semi-pure **[6-Et₂O][BArF]** as a fluffy yellow powder. Yield: 24.1 mg (63%). The compound was not sufficiently stable for crystallization or

further purification, but identification was confirmed by comparison of spectroscopic data to those of [6-DMAP][OTf] and **6-OTf.** ¹H NMR (CD₂Cl₂, 400 MHz) [NOTE: Integrations are estimated for aliphatic signals due to presence of impurities]: δ 7.93–7.88 (m, 2H), 7.65–7.52 (m, 6H), 4.18 (q, ${}^{3}J_{HH} = 7.0 \text{ Hz}$, 4H, O(CH₂CH₃)₂), 2.64–2.52 (m, 2H), 2.32–2.21 (m, 4H), 2.01 (t, J = 14.1 Hz, 4H), 1.94-1.80 (m, 10H), 1.76-1.66 (m, 8H),1.63–1.51 (m, 8H), 1.49–1.07 (m, 18H), 1.37 (t, ${}^{3}J_{HH} = 7.0 \text{ Hz}$, 6H, $O(CH_2CH_3)_2$). ¹³C{¹H} NMR (CD₂Cl₂, 101 MHz): For cation portion only: δ 141.2 (t, J = 16 Hz), 139.2 (t, J = 9.3 Hz), 135.0 (t, J = 5.5 Hz), 133.3, 132.3, 130.4, 73.1, 38.4 (t, J = 10Hz), 33.4 (t, J = 12 Hz), 32.7, 28.9–28.3 (m), 28.2, 28.1 (t, J =5.1 Hz), 27.5, 27.2–26.9 (m), 26.7, 26.1, 13.3. ¹⁹F{¹H} NMR $(CD_2Cl_2, 376 \text{ MHz}): \delta -133.22, -164.01 \text{ (t, } J = 20.6 \text{ Hz)}, -164.01 \text{ (t, } J = 20.6 \text{$ 167.83 (t, J = 18.9 Hz). ²⁹Si{¹H} NMR (CD₂Cl₂, 80 MHz): δ – 25.8 (t, ${}^{3}J_{PSi} = 7.4 \text{ Hz}$). ${}^{31}P\{{}^{1}H\}$ NMR (CD₂Cl₂, 162 MHz): δ 39.0 (${}^{1}J_{PRh} = 124 \text{ Hz}$). IR (CH₂Cl₂, cm⁻¹): v 1970 (CO).

Method B. Complex **1-OTf** (35.6 mg, 0.039 mmol) was dissolved in dichloromethane (1 mL), and a solution of LiB(C_6F_5)₄·2.5Et₂O (22 mg, 0.026 mmol) in dichloromethane (2 mL) was added to it with stirring. The reaction was allowed to proceed 5 min, and the volume of the reaction was reduced to ca. 1 mL *in vacuo*. The entire mixture was transferred to a J Young NMR tube, subjected to one freeze–pump–thaw cycle, and the headspace evacuated and backfilled with CO₂ (1 atm). The reaction was allowed to proceed overnight, affording [6-Et₂O][BArF] in 67% purity, as judged by ³¹P NMR spectroscopy.

Ph₃Si–Rh(PMe₃)₃ (7). Complex 7 was prepared according to published methods.²⁵ Since NMR data are not available in the original report of 7, we include them here and reproduce them in the Supporting Information. ¹H NMR (C₆D₆, 400 MHz): δ 8.17 (dd, $J_1 = 8.0$ Hz, $J_2 = 1.5$ Hz, 6H), 7.28 (m, 6H), 7.18 (tt, $J_1 = 7.3$ Hz, $J_2 = 1.6$ Hz, 3H), 0.95 (br m, 27H). ²⁹Si{¹H} NMR (C₆D₆, 80 MHz): δ 12.2 (dq, ${}^1J_{RhSi} = 42$ Hz, ${}^2J_{PSi} = 28$ Hz). ³¹P{ 1 H} NMR (C₆D₆, 162 MHz): δ –18.1 (br d, ${}^1J_{RhP} = 141$ Hz).

Ph₃SiO-Rh(PMe₃)₂(CO) (8). Complex 7 (41 mg, 0.069 mmol) was dissolved in C₆D₆ (0.7 mL) and transferred to a J Young NMR tube. The solution was subjected to one freezepump-thaw cycle and the headspace was backfilled with CO2 (1 atm). The reaction proceeded immediately upon warming, as indicated by a color change from red to yellow. Quantitative conversion to 8 after 5 min was confirmed by ¹H NMR spectroscopy. Volatiles were removed in vacuo to afford 8 as a yellow powder. Complex 8 was unstable for extended periods in the absence of added PMe₃, so microanalysis of the product was not obtained. NMR spectra of 8 (except ³¹P) were obtained prior to workup, in the presence of PMe₃ (1 equiv). ¹H NMR (C₆D₆, 400 MHz): δ 8.05 (dd, $J_1 = 7.9$ Hz, $J_2 = 1.5$ Hz, 6H), 7.32–7.26 (m, 6H), 7.26-7.21 (m, 3H), 0.90 (br s, 27H: bound and free PMe₃). ${}^{13}C\{{}^{1}H\}$ NMR (C₆D₆, 101 MHz): δ 191.8 (d, ${}^{2}J_{RhC} = 67$ Hz, Rh-CO), 142.6, 136.2, 128.6, 127.6, 16.2 (br, P-CH₃). $^{29}Si\{^1H\}$ NMR (C₆D₆, 80 MHz): δ –26.4 (s). $^{31}P\{^1H\}$ NMR $(C_6D_6, 162 \text{ MHz}): \delta -13.1 \text{ (d, }^1J_{RhP} = 121 \text{ Hz}). \text{ IR (CH}_2\text{Cl}_2,$ cm^{-1}): v 1950 (CO).

[(^{Cy}P₂Si^(OH)(µ-OH))Rh(CO)][OTf] (9-OTf). Complex 6-OTf (15 mg, 0.018 mmol) was dissolved in dichloromethane (1 mL) and a solution of water (1 mL, 0.028 M in CH₂Cl₂) was added slowly with stirring. The reaction was allowed to proceed for 10 min, after which quantitative conversion to 9-OTf was confirmed by ³¹P NMR spectroscopy. Most volatiles were removed *in vacuo* (note: the material was unstable to extended vacuum)

and the resulting material was redissolved and recrystallized from a minimal amount of diethyl ether at -35 °C to afford 9-**OTf** as yellow crystals. Crystals suitable for X-ray diffraction analysis were obtained from a concentrated solution of 9-OTf in benzene at ambient temperature. Since 9-OTf was unstable to extended vacuum, residual solvent could not be entirely removed and precise isolated yields were not obtained. ¹H NMR $(C_6D_6, 400 \text{ MHz})$: δ 10.93 (s, 1H), 8.18 (d, J = 6.9 Hz, 2H), 7.13–7.00 (m, 6H), 6.78 (s, 1H), 2.47–2.24 (m, 6H), 1.93 (d, J = 12.6 Hz, 2H), 1.88–1.31 (m, 26H), 1.22–1.01 (m, 10H). $13C\{1H\}$ NMR (C6D6, 101 MHz): δ 194.4 (dt, 1JRhC = 81 Hz, 2JPC = 14 Hz, Rh–CO), 143.6 (t, J = 10 Hz), 138.0 (t, J = 6.2Hz), 135.6 (t, J = 18 Hz), 131.1, 130.0, 129.8, 38.5 (t, J = 9.9Hz), 33.2-32.8 (m), 28.2, 27.5-27.3 (m), 27.1 (t, J = 5.1 Hz), 26.9–26.6 (m), 26.2, 25.9. ¹⁹F{¹H} NMR (CD₂Cl₂, 376 MHz): $\delta - 77.8.^{29}Si\{^{1}H\}$ NMR (CD₂Cl₂, 80 MHz): No ²⁹Si signal was located for this compound. ³¹P{¹H} NMR (CD₂Cl₂, 162 MHz): δ 38.9 (${}^{1}J_{PRh}$ = 119 Hz). IR (CH₂Cl₂, cm⁻¹): ν 3346 (OH), 2235 (OH), 1980 (CO). NOTE: Complex 9-OTf is unstable to vacuum, so drying for suitable microanalysis was not possible.

(CyP2SiOBpin)Rh(H)(CO)(OTf) (10-OTf). Complex 6-OTf (20 mg, 0.023 mmol) was dissolved in 1:1 dichloromethane/benzene (2 mL), and a solution of pinacolborane (121 μL, 0.19 M in fluorobenzene, 0.023 mmol) was added with stirring. The reaction mixture was heated in a sealed vial at 60 °C for 2 h. Volatiles were removed in vacuo to afford a yellow powder, which was washed with cold pentane (3 × 2 mL) and dried in vacuo. Analytically pure 10-OTf was obtained by crystallization from ether/pentane vapor cross-diffusion at -35 °C. X-ray quality crystals were obtained in the same manner. Yield: 9.1 mg (40%). ¹H NMR (C₆D₆, 400 MHz): δ 8.18 (d, J = 7.0Hz, 2H), 7.52 (dt, $J_1 = 6.9$ Hz, $J_2 = 3.1$ Hz, 2H), 7.19 (tq, $J_1 =$ 7.4 Hz, $J_2 = 1.3$ Hz, 2H), 7.10 (tq, $J_1 = 7.4$ Hz, $J_2 = 1.4$ Hz, 2H), 3.16-3.06 (m, 2H), 2.46-2.33 (m, 4H), 2.20-2.04 (m, 6H), 1.87 (d, J = 11.8 Hz, 2H), 1.77-1.39 (m, 20H), 1.37-1.15 (m, 6H),1.09-0.95 (m, 4H), 0.88 (s, 12H, -CH3 from Bpin), -8.60 (dt, ${}^{1}J_{RhH} = 12.2 \text{ Hz}, {}^{2}J_{PH} = 9.6 \text{ Hz}, 1H, Rh-H). {}^{11}B\{{}^{1}H\} \text{ NMR}$ $(C_6D_6, 128 \text{ Hz})$: $\delta 20.4 \text{ (br s)}$. $^{13}C\{^1H\}$ NMR $(C_6D_6, 101 \text{ MHz})$: δ 153.8 (td, J_1 = 22 Hz, J_2 = 4.7 Hz), 142.2 (td, J_1 = 24 Hz, J_2 = 4.0 Hz), 133.3 (t, J = 9.7 Hz), 130.03, 129.99, 129.3 (t, J = 3.5Hz), 82.1, 36.3 (t, J = 12 Hz), 34.4 (t, J = 12 Hz), 30.2, 29.1, 28.5, 27.9 (t, J = 4.9 Hz), 27.5, 27.1 (dt, $J_1 = 12$ Hz, $J_2 = 6.6$ Hz), 26.9, 26.7 (t, J = 6.6 Hz), 26.4, 24.6. ¹⁹F{¹H} NMR $(CD_2Cl_2, 376 \text{ MHz}): \delta -76.9. ^{29}Si\{^1H\} \text{ NMR } (CD_2Cl_2, 80)$ MHz): 36.3 (dt, ${}^{1}J_{RhSi} = 35$ Hz, ${}^{2}J_{PSi} = 3.9$ Hz). ${}^{31}P\{{}^{1}H\}$ NMR (CD₂Cl₂, 162 MHz): δ 72.3 (${}^{1}J_{PRh}$ = 108 Hz). IR (CH₂Cl₂, cm⁻ 1): 2082 (CO), 1988 (Rh-H). Anal. calcd. for C₄₄H₆₅BF₃O₇P₂RhSSi: C, 52.91; H, 6.56. Found: C, 52.67; H, 6.46.

X-ray Crystallography. Single-crystal X-ray diffraction data for **6-OTf**, **[6-DMAP][OTf]**, **9-OTf**, and **10-OTf** were collected on a Rigaku XtaLAB mini diffractometer using Mo K α radiation (λ = 0.71073 Å). The diffractometer was equipped with an Oxford Cryosystems desktop cooler (Oxford Cryosystems Ltd, Oxford) for low-temperature data collection. The crystals were mounted on a MiTeGen micromount (MiTeGen, LLC, Ithaca, NY) using STP oil. The frames were integrated using CrystalClear-SM Expert 3.1 b27⁴² to give the *hkl* files corrected for *Lp* and decay. Data were corrected for absorption effects using a multiscan method (REQAB).

All structures were solved using SHELXS-2013 and refined using SHELXL-2013 with the Olex2 software package.⁴³ All

non-hydrogen atoms were refined with anisotropic thermal parameters. Ruthenium and silicon hydrides were located in the Fourier difference maps and refined isotropically; all other hydrogen atoms were inferred geometrically from neighboring sites and refined with riding thermal parameters. Crystallographic parameters of all complexes are summarized in Table S1. ORTEP drawings were prepared using ORTEP-3 for Windows V2013.1⁴⁴ and POV-Ray for Windows v3.6.⁴⁵ Crystallographic data for the complexes have been deposited at the Cambridge Crystallographic Data Centre (Nos. 1911566–1911569) and can be obtained free of charge via www.ccdc.cam.ac.uk.

Special Crystallographic Refinement Details. The crystals obtained for 6-OTf diffracted poorly and yielded a low-quality structure. Although connectivity was well established for 6-OTf and the structure was further corroborated by the high-quality dataset for the related [6-DMAP][OTf], the low quality of the data only permitted anisotropic refinement for Rh, Si, P, and S atoms in 6-OTf.

ASSOCIATED CONTENT

Supporting Information

The Supporting Information is available free of charge on the ACS Publications website.

Tabulated X-ray parameters, NMR and IR spectra, computational details and energies of all computed structures (PDF)

Coordinates of all computed structures (XYZ)

Crystallographic information (CIF)

AUTHOR INFORMATION

Corresponding Authors

- * E-mail: mwhited@carleton.edu (M.T.W.).
- * E-mail: taylorb@up.edu (B.L.H.T.).

ORCID

Matthew T. Whited: 0000-0002-1193-9078 Paul O. Peterson: 0000-0002-0602-2695 Daron E. Janzen: 0000-0002-5584-1961 Buck L. H. Taylor: 0000-0002-6586-3865

Notes

The authors declare no competing financial interests.

ACKNOWLEDGMENT

This material is based upon work supported by a CAREER award from the National Science Foundation (CHE-1552591 to M.T.W.). NMR spectroscopy and X-ray crystallography were enabled by NSF-MRI grants 1428752 and 1125975, respectively. Computational resources were provided by an NSF-MRI award (CHE-1039925) through the Midwest Undergraduate Computational Chemistry Consortium (MU3C), as well as the Extreme Science and Engineering Discovery Environment (XSEDE), which is supported by NSF award ACI-1548562. M.T.W. is a Henry Dreyfus Teacher-Scholar. J.Z. was supported by the Riecker Endowed Fund for the Sciences at Carleton College.

REFERENCES

- (1) Stephan, D. W.; Erker, G. Frustrated Lewis Pair Chemistry: Development and Perspectives. *Angew. Chem., Int. Ed.* **2015**, *54*, 6400-6441.
- (2) Hartwig, J. F. Organotransition Metal Chemistry: From Bonding to Catalysis; University Science Books: Sausalito, CA, 2010.
- (3) Hazari, N.; Heimann, J. E. Carbon Dioxide Insertion into Group 9 and 10 Metal-Element σ Bonds. *Inorg. Chem.* **2017**, *56*, 13655-13678.
- (4) (a) Zhang, J.; Foley, B. J.; Bhuvanesh, N.; Zhou, J.; Janzen, D. E.; Whited, M. T.; Ozerov, O. V. Synthesis and Reactivity of Pincer-Type Cobalt Silyl and Silylene Complexes. Organometallics 2018, 37, 3956-3962. (b) Whited, M. T.; Zhang, J.; Ma, S.; Nguyen, B. D.; Janzen, D. E. Silylene-Assisted Hydride Transfer to CO2 and CS2 at a [P₂Si]Ru Pincer-Type Complex. *Dalton Trans.* **2017**, *46*, 14757-14761. (c) Whited, M. T.; Deetz, A. M.; Donnell, T. M.; Janzen, D. E. Examining the Role of Rh/Si Cooperation in Alkene Hydrogenation by a Pincer-Type [P₂Si]Rh Complex. Dalton Trans. 2016, 45, 9758-9761. (d) Whited, M. T.; Deetz, A. M.; Boerma, J. W.; DeRosha, D. E.; Janzen, D. E. Formation of Chlorosilyl Pincer-Type Rhodium Complexes by Multiple Si-H Activations Bis(phosphine)/Dihydrosilyl Ligands. Organometallics 2014, 33, 5070-5073. (e) Whited, M. T. Metal-Ligand Multiple Bonds as Frustrated Lewis Pairs for C-H Functionalization. Beilstein J. Org. Chem. 2012, 8, 1554-1563.
- (5) (a) Campion, B. K.; Heyn, R. H.; Tilley, T. D. Carbon Dioxide Activation by a Transition-Metal–Silicon Bond. Formation of Silanecarboxylate Complexes Cp₂Sc(μ-O₂CSiR₃)₂. *Inorg. Chem.* **1990**, 29, 4355-4356. (b) Mukherjee, D.; Lampland, N. L.; Yan, K. K.; Dunne, J. F.; Ellern, A.; Sadow, A. D. Divergent Reaction Pathways of Tris(oxazolinyl)borato Zinc and Magnesium Silyl Compounds. *Chem. Commun.* **2013**, 49, 4334-4336. (c) Kleeberg, C.; Cheung, M. S.; Lin, Z. Y.; Marder, T. B. Copper-Mediated Reduction of CO₂ with pinB–SiMe₂Ph via CO₂ Insertion into a Copper-Silicon Bond. *J. Am. Chem. Soc.* **2011**, *133*, 19060-19063. (d) Witzke, R. J.; Tilley, T. D. A Two-Coordinate Ni(I) Silyl Complex: CO₂ Insertion and Oxidatively-Induced Silyl Migrations. *Chem. Commun.* **2019**, *55*, 6559-6562.
- (6) A photoinduced anomalous insertion of an aldehyde into an FeSi bond has been reported, though the mechanism is not entirely clear: Vargas, R. M.; Hossain, M. M. Photochemical Reactions of $(\eta^5 C_5H_5)Fe(CO)_2SiMe_2R$ (R = Me, Ph) with ArCHO (Ar = C_6H_5 , p-OCH $_3C_6H_4$). *Inorg. Chim. Acta* **1993**, *204*, 139-140.
- (7) Anomalous insertion of ketones and aldehydes into M-Si bonds has been proposed as a key step in some hydrosilylations: (a) Ojima, I.; Kogure, T.; Kumagai, M.; Horiuchi, S.; Sato, T. Reduction of Carbonyl Compounds via Hydrosilylation: 2. Asymmetric Reduction of Ketones via Hydrosilylation Catalyzed by a Rhodium(I) Complex with Chiral Phosphine Ligands. *J. Organomet. Chem.* 1976, 122, 83-97. (b) Ito, J.; Hosokawa, S.; Khalid, H. B.; Nishiyama, H. Preparation, Characterization, and Catalytic Reactions of NCN Pincer Iron Complexes Containing Stannyl, Silyl, Methyl, and Phenyl Ligands. *Organometallics* 2015, 34, 1377-1383.
- (8) (a) Vigalok, A.; BenDavid, Y.; Milstein, D. Complexation of N₂, H₂, CO₂, and Ethylene to a T-Shaped Rhodium(I) Core. *Organometallics* **1996**, *15*, 1839-1844. (b) Kaska, W. C.; Nemeh, S.; Shirazi, A.; Potuznik, S. Reduction of Carbon Dioxide by {2,6-Bis[(ditert-butylphosphino)methyl]phenyl} dihydridorhodium(III). *Organometallics* **1988**, *7*, 13-15.
- (9) Whited, M. T.; Trenerry, M. J.; DeMeulenaere, K. E.; Taylor, B. L. H. Computational and Experimental Investigation of Alkene Hydrogenation by a Pincer-Type [P₂Si]Rh Complex: Alkane Release via Competitive σ-Bond Metathesis and Reductive Elimination. *Organometallics* **2019**, *38*, 1493-1501.
- (10) Goikhman, R.; Milstein, D. Reactivity of Rhodium-Triflate Complexes with Diphenylsilane: Evidence for Silylene Intermediacy in Stoichiometric and Catalytic Reactions. *Chem. Eur. J.* **2005**, *11*, 2983-2088
- (11) Other examples of pincer-type complexes featuring a siloxide donor: (a) Stobart, S. R.; Zhou, X. B.; Cea-Olivares, R.; Toscano, A. Activation of Water and of Dioxygen by a Bis(diphenylphosphinopropyl)silyl (biPSi) Complex of Ruthenium(II):

- Formation of Bis(diphenylphosphinopropyl)siloxo Cage Complexes. Concomitant Oxygen Atom Insertion into a Silicon—Carbon Bond. *Organometallics* **2001**, *20*, 4766-4768. (b) Korshin, E. E.; Leitus, G.; Shimon, L. J. W.; Konstantinovski, L.; Milstein, D. Silanol-Based Pincer Pt(II) Complexes: Synthesis, Structure, and Unusual Reactivity. *Inorg. Chem.* **2008**, *47*, 7177-7189. (c) Murphy, L. J.; Ruddy, A. J.; McDonald, R.; Ferguson, M. J.; Turculet, L. Activation of Molecular Hydrogen and Oxygen by PSiP Complexes of Cobalt. *Eur. J. Inorg. Chem.* **2018**, 4481-4493.
- (12) (a) Marciniec, B.; Blazejewska-Chadyniak, P.; Kubicki, M. Synthesis, First Structures, and Catalytic Activity of the Monomeric Rhodium(I)–Siloxide Phosphine Complexes. *Can. J. Chem.* **2003**, *81*, 1292-1298. (b) Smith, D. A.; Herbert, D. E.; Walensky, J. R.; Ozerov, O. V. Monomeric Rhodium(II) Complexes Supported by a Diarylamido/Bis(phosphine) PNP Pincer Ligand and Their Reactivity Toward Dihydrogen. *Organometallics* **2013**, *32*, 2050-2058.
- (13) Thompson, C. V.; Arman, H. D.; Tonzetich, Z. J. Square-Planar Iron(II) Silyl Complexes: Synthesis, Characterization, and Insertion Reactivity. *Organometallics* **2019**, *38*, 2979-2989.
- (14) Veige, A. S.; Wolczanski, P. T.; Lobkovsky, E. B. (silox)₃RePMe₃ (silox = 'Bu₃SiO) is Carbonylated to the Double Insertion Product (silox)(Me₃P){cis-(CO)₂}Re{trans-(CO₂Si'Bu₃)₂}. Chem. Commun. **2001**, 2734-2735.
- (15) Whited, M. T.; Grubbs, R. H. Oxygen-Atom Transfer from Carbon Dioxide to a Fischer Carbene at (PNP)Ir. *J. Am. Chem. Soc.* **2008**, *130*, 5874-5875.
- (16) Bedford, R. B.; Hill, A. F.; White, A. J. P.; Williams, D. J. Cycloadditions of Ruthenium Alkylidyne Complexes with Carbonyl or Thiocarbonyl Compounds. *Angew. Chem., Int. Ed.* **1996**, *35*, 95-97.
- (17) Litz, K. E.; Henderson, K.; Gourley, R. W.; Holl, M. M. B. Reversible Insertion Reactions of a Platinum Germylene Complex. *Organometallics* **1995**, *14*, 5008-5010.
- (18) Mitchell, G. P.; Tilley, T. D. Reversible Cycloaddition of Isocyanates to Ruthenium Silylene Complexes. *J. Am. Chem. Soc.* **1997**, *119*, 11236-11243.
- (19) Whited, M. T.; Trenerry, M. J.; DeMeulenaere, K. E.; Taylor, B. L. H. Computational and Experimental Investigation of Alkene Hydrogenation by a Pincer-Type [P₂Si]Rh Complex: Alkane Release via Competitive σ-Bond Metathesis and Reductive Elimination. *Organometallics* **2018**, *38*, 1493-1501.
- (20) The instability of $1-Et_2O^+$ and $4-Et_2O^+$ precluded a rigorous comparison with the other complexes, but $1-Et_2O^+$ reacted with CO₂ at a qualitatively similar rate to $1-DMAP^+$ and 1-OTf.
- (21) Unlike related complexes in the series, 1-CH₃ underwent a clean reaction with CO₂ in bromobenzene to afford an as-yet unidentified product that is not an analogue of 6-OTf.
- (22) (a) Rohmann, K.; Holscher, M.; Leitner, W. Can Contemporary Density Functional Theory Predict Energy Spans in Molecular Catalysis Accurately Enough To Be Applicable for in Silico Catalyst Design? A Computational/Experimental Case Study for the Ruthenium-Catalyzed Hydrogenation of Olefins. *J. Am. Chem. Soc.* **2016**, *138*, 433-443. (b) Ostapowicz, T. G.; Holscher, M.; Leitner, W. CO₂ Insertion into Metal-Carbon Bonds: A Computational Study of Rh^I Pincer Complexes. *Chem. Eur. J.* **2011**, *17*, 10329-10338.
- (23) Rossi, A. R.; Hoffmann, R. Transition-Metal Pentacoordination. *Inorg. Chem.* **1975**, *14*, 365-374.
- (24) Tan, G.; Blom, B.; Gallego, D.; Irran, E.; Driess, M. Elucidating the Effect of the Nucleophilicity of the Silyl Group in the Reduction of CO₂ to CO Mediated by Silyl-Copper(I) Complexes. *Chem. Eur. J.* **2014**, *20*, 9400-9408.
- (25) Thorn, D. L.; Harlow, R. L. Structure and Reactivity of a (Triphenylsilyl)rhodium(I) Compound. *Inorg. Chem.* **1990**, *29*, 2017-2019.
- (26) Kallane, S. I.; Braun, T.; Teltewskoi, M.; Braun, B.; Herrmann, R.; Laubenstein, R. Remarkable Reactivity of a Rhodium(I) Boryl Complex Towards CO₂ and CS₂: Isolation of a Carbido Complex. *Chem. Commun.* **2015**, *51*, 14613-14616.
- (27) (a) Ariafard, A.; Brookes, N. J.; Stranger, R.; Yates, B. F. DFT Study on the Mechanism of the Activation and Cleavage of CO₂ by (NHC)CuEPh₃ (E = Si, Ge, Sn). *Organometallics* **2011**, *30*, 1340-1349. (b) Zhao, H. T.; Lin, Z. Y.; Marder, T. B. Density Functional Theory

- Studies on the Mechanism of the Reduction of CO₂ to CO Catalyzed by Copper(I) Boryl Complexes. *J. Am. Chem. Soc.* **2006**, *128*, 15637-15643
- (28) Garcia-Camprubi, A.; Martin, M.; Sola, E. Addition of Water Across Si–Ir Bonds in Iridium Complexes with κ-*P*,*P*,*Si* (biPSi) Pincer Ligands. *Inorg. Chem.* **2010**, *49*, 10649-10657.
- (29) Davidson, J. J.; Nagaraja, C. M.; Chen, C. H.; Foxman, B. M.; Ozerov, O. V. Palladium Complexes of a New Phosphine-Amido-Siloxide Pincer Ligand with Variable Degrees of Protonation. *Inorg. Chim. Acta* **2014**, *422*, 70-77.
- (30) Hadlington, T. J.; Szilvasi, T.; Driess, M. Synthesis of a Metallo-Iminosilane via a Silanone–Metal π -Complex. *Angew. Chem., Int. Ed.* **2017**, *56*, 14282-14286.
- (31) (a) Vol'pin, M. E.; Kolomnikov, I. S. In *Coordination Chemistry-XIV*; Lever, A. B. P., Ed.; Butterworth-Heinemann: London, 1973, p 567-581. (b) Schneck, F.; Ahrens, J.; Finger, M.; Stuckl, A. C.; Wurtele, C.; Schwarzer, D.; Schneider, S. The Elusive Abnormal CO₂ Insertion Enabled by Metal-Ligand Cooperative Photochemical Selectivity Inversion. *Nat. Commun.* **2018**, *9*.
- (32) (a) Dang, L.; Lin, Z. Y.; Marder, T. B. Boryl Ligands and their Roles in Metal-Catalysed Borylation Reactions. *Chem. Commun.* **2009**, 3987-3995. (b) Dang, L.; Lin, Z. Y.; Marder, T. B. DFT Studies on the Carboxylation of Arylboronate Esters with CO₂ Catalyzed by Copper(I) Complexes. *Organometallics* **2010**, *29*, 917-927.
- (33) Laitar, D. S.; Muller, P.; Sadighi, J. P. Efficient Homogeneous Catalysis in the Reduction of CO₂ to CO. *J. Am. Chem. Soc.* **2005**, *127*, 17196-17197.
- (34) Ahrens, T.; Schmiedecke, B.; Braun, T.; Herrmann, R.; Laubenstein, R. Activation of CS₂ and COS at a Rhodium(I) Germyl Complex: Generation of CS and Carbido Complexes. *Eur. J. Inorg. Chem.* **2017**, 713-722.
- (35) Krogman, J. P.; Foxman, B. M.; Thomas, C. M. Activation of CO₂ by a Heterobimetallic Zr/Co Complex. *J. Am. Chem. Soc.* **2011**, *133*, 14582-14585.
- (36) Leitl, J.; Marquardt, M.; Coburger, P.; Scott, D. J.; Streitferdt, V.; Gschwind, R. M.; Muller, C.; Wolf, R. Facile C=O Bond Splitting of Carbon Dioxide Induced by Metal-Ligand Cooperativity in a Phosphinine Iron(0) Complex. *Angew. Chem., Int. Ed.*
- (37) Frisch, M. J.; Trucks, G. W.; Schlegel, H. B.; Scuseria, G. E.; Robb, M. A.; Cheeseman, J. R.; Scalmani, G.; Barone, V.; Mennucci, B.; Petersson, G. A.; Nakatsuji, H.; Caricato, M.; Li, X.; Hratchian, H. P.; Izmaylov, A. F.; Bloino, J.; Zheng, G.; Sonnenberg, J. L.; Hada, M.; Ehara, M.; Toyota, K.; Fukuda, R.; Hasegawa, J.; Ishida, M.; Nakajima, T.; Honda, Y.; Kitao, O.; Nakai, H.; Vreven, T.; Montgomery Jr., J. A.; Peralta, J. E.; Ogliaro, F.; Bearpark, M. J.; Heyd, J.; Brothers, E. N.; Kudin, K. N.; Staroverov, V. N.; Kobayashi, R.; Normand, J.; Raghavachari, K.; Rendell, A. P.; Burant, J. C.; Iyengar, S. S.; Tomasi, J.; Cossi, M.; Rega, N.; Millam, N. J.; Klene, M.; Knox, J. E.; Cross, J. B.; Bakken, V.; Adamo, C.; Jaramillo, J.; Gomperts, R.; Stratmann, R. E.; Yazyev, O.; Austin, A. J.; Cammi, R.; Pomelli, C.; Ochterski, J. W.; Martin, R. L.; Morokuma, K.; Zakrzewski, V. G.; Voth, G. A.; Salvador, P.; Dannenberg, J. J.; Dapprich, S.; Daniels, A. D.; Farkas, Ö.; Foresman, J. B.; Ortiz, J. V.; Cioslowski, J.; Fox, D. J. Gaussian 09, Gaussian, Inc.: Wallingford, CT, USA, 2009.
- (38) Legault, C. Y. *CYLView*, 1.0b; Université de Sherbrooke: Canada, 2009.
- (39) Andrienko, G. A. ChemCraft V1.8 (build 562) at http://www.chemcraftprog.com,
- (40) (a) Grimme, S. Semiempirical GGA-Type Density Functional Constructed with a Long-Range Dispersion Correction. *J. Comput. Chem.* **2006**, *27*, 1787-1799. (b) Grimme, S.; Ehrlich, S.; Goerigk, L. Effect of the Damping Function in Dispersion Corrected Density Functional Theory. *J. Comput. Chem.* **2011**, *32*, 1456-1465.
- (41) (a) Weigend, F.; Ahlrichs, R. Balanced Basis Sets of Split Valence, Triple Zeta Valence and Quadruple Zeta Valence Quality for H to Rn: Design and Assessment of Accuracy. *Phys. Chem. Chem. Phys.* **2005**, 7, 3297-3305. (b) Weigend, F. Accurate Coulomb-Fitting Basis Sets for H to Rn. *Phys. Chem. Chem. Phys.* **2006**, 8, 1057-1065.
- (42) CrystalClear, Rigaku Americas and Rigaku: The Woodlands, TX, 2011.

- (43) Dolomanov, O. V.; Bourhis, L. J.; Gildea, R. J.; Howard, J. A. K.; Puschmann, H. OLEX2: A Complete Structure Solution, Refinement and Analysis Program. *J. Appl. Cryst.* **2009**, *42*, 339-341. (44) Farrugia, L. J. WinGX and ORTEP for Windows: An Update. *J. Appl. Cryst.* **2012**, *45*, 849-854.
- (45) Persistence of Vision Raytracer (Version 3.6), Persistence of Vision Pty. Ltd.: 2004.

